

# **Tau, XMAP215/Msps and Eb1 jointly regulate microtubule polymerisation and bundle formation in axons**

Ines Hahn<sup>#, 1</sup>, Andre Voelzmann<sup>1</sup>, Jill Parkin<sup>1</sup>, Judith Fuelle<sup>1</sup>, Paula G Slater<sup>2</sup>, Laura A Lowery<sup>3</sup>, Natalia Sanchez-Soriano<sup>#†4</sup> & Andreas Prokop<sup>#†1</sup>

1) The University of Manchester, Manchester Academic Health Science Centre, Faculty of Biology, Medicine and Health, School of Biology, Manchester, UK

2) Department of Biology, Boston College, Chestnut Hill, MA, USA

3) Department of Medicine, Boston University Medical Center, Boston, MA, USA

4) Department of Molecular Physiology & Cell Signalling, Institute of Systems, Molecular & Integrative Biology, University of Liverpool, Liverpool, United Kingdom

**Running title:** Tau, XMAP215 and Eb1, a functional trio for microtubule polymerisation and organisation

**Key words:** *Drosophila*, neurodegeneration, axons, cytoskeleton, microtubules

<sup>#</sup> authors for correspondence:

The University of Manchester

Faculty of Life Sciences

Oxford Road

Manchester M13 9PT

Tel: +44-(0)161-27-51556

Fax: +44-(0)161-27-51505

[Ines.Hahn@manchester.ac.uk](mailto:Ines.Hahn@manchester.ac.uk)

[N.Sanchez-Soriano@liverpool.ac.uk](mailto:N.Sanchez-Soriano@liverpool.ac.uk)

[Andreas.Prokop@manchester.ac.uk](mailto:Andreas.Prokop@manchester.ac.uk)

<sup>†</sup> joined senior authors

## **Summary statement:**

Eb1, XMAP215 and tau operate as a functional unit in axons to promote the polymerisation of microtubules and their organisation into the parallel bundles essential for axonal transport.

## **Abstract**

Axons are the enormously long cable-like cellular processes of neurons that wire nervous systems and have to survive for up to a century in humans. We lose ~40% of axons towards high age and far more in neurodegenerative diseases. Sustaining axons requires axonal transport and dynamic morphogenetic changes, both crucially dependent on bundles of microtubules that run all along axons. How polymerisation is regulated to form, repair and

replace microtubules in these bundles during axon development and maintenance is virtually unknown. Here, we show in axons of *Drosophila* and *Xenopus* neurons alike that Eb1, XMAP215/Msps and Tau are key players which operate as one functional unit to promote microtubule polymerisation. Eb1 and XMAP215/Msps are interdependent core factors at the microtubule tip, whereas Tau outcompetes Eb1 binding at microtubule lattices, thus preventing its pool depletion at polymerising plus ends. In agreement with their closely interwoven functions, the three factors show the same combination of axonal loss-of-function mutant phenotypes including: (1) reduced microtubule polymerisation dynamics and shorter axon growth, indicating their importance for upholding microtubule mass in axons; (2) prominent deterioration of parallel microtubule bundles into disorganised curled conformations, indicating their key roles in promoting essential axonal architecture. We show the latter to occur through Eb1- and spectraplakins-dependent guidance of extending microtubules. We conclude that Eb1, XMAP215/Msps and Tau jointly promote microtubule polymerisation, important to regulate the quantity and bundled organisation of microtubules and offering new ways to think about developmental and degenerative axon pathologies and how to treat them.

## Introduction

Axons are the enormously long cable-like cellular processes of neurons that wire nervous systems. In humans, axons of  $\leq 15\mu\text{m}$  diameter can be up to a meter long (Prokop, 2020). They are constantly exposed to mechanical challenges, yet have to survive for up to a century; we lose ~40% of axons towards high age and far more in neurodegenerative diseases (Adalbert & Coleman, 2012, Calkins, 2013, Marner, Nyengaard et al., 2003).

Their growth and maintenance require parallel bundles of microtubules (MTs) that run all along axons, providing the highways for life-sustaining transport and driving morphogenetic events. Consequently, bundle decay through MT mass decrease and/or MT disorganisation is a common feature in axon pathologies (summarised in (Hahn, Voelzmann et al., 2019). Key roles must be played by MT polymerisation, which is not only essential for the *de novo* formation of MT bundles during axon growth occurring in development, plasticity or regeneration, but also to repair and replace senescent MTs during long-term maintenance (Gasic & Mitchison, 2019, Schaedel, John et al., 2015, Voelzmann, Hahn et al., 2016). However, the molecular mechanisms driving MT polymerisation in axons are surprisingly little understood.

*In vitro*, MTs undergo polymerisation in the absence of enzymatic catalysis, but the addition of factors such as CLASPs, stathmins, tau, Eb proteins or XMAP215 can enhance and refine the process (Aher, Rai et al., 2020, Al-Bassam, Kim et al., 2010, Brouhard, Stear et al., 2008, Drechsel, Hyman et al., 1992, Li, Moriwaki et al., 2012, Manna, Thrower et al., 2009, Zanic, Widlund et al., 2013). Accordingly, many candidate regulators have been proposed in the literature to regulate MT polymerisation in axons, comprising factors that are MT plus end-associating, MT shaft-binding or involved in tubulin provision (summarised in (Voelzmann et al., 2016). We would therefore expect that MT polymerisation in axons is regulated through functional networks of proteins, but we are far from understanding what the key players are and how they are regulated by other proteins in these networks.

To gain such knowledge, we have chosen *Drosophila* primary neurons as one consistent model amenable to combinatorial genetics as a powerful strategy to decipher complex regulatory networks (Prokop, Beaven et al., 2013). Our previous loss-of-function studies of 9 MT plus end-associating factors in these *Drosophila* neurons (CLASP, CLIP190, dynein heavy chain, APC, p150<sup>Glued</sup>, Eb1, Short stop/Shot, doublecortin, Lis1) have taken axon length as a crude proxy



readout for net polymerisation, mostly revealing relatively mild axon length phenotypes, with the exception of Eb1 and Shot which cause severe axon shortening {Beaven, 2015 #6487; Sánchez-Soriano, 2009 #7139; Alves-Silva, 2012 #4930; A.V., unpublished data}.

Here we have taken these analyses to the next level. We show that three factors, Eb1, XMAP215/Msps and Tau, share a unique combination of mutant phenotypes, including reduced axonal MT polymerisation in frog and fly neurons in culture and *in vivo*. Our data reveal that the three factors operate as a functional unit: whereas Eb1 and XMAP215/Msps act interdependently at MT plus ends, Tau outcompetes Eb1 binding at MT lattices, thus preventing its pool depletion at polymerising MT plus ends. By upholding MT polymerisation, this functional trio also promotes the bundle conformation of axonal MTs through a guidance mechanism mediated by the spectraplakins Shot.

## Methods

### Fly stocks

Loss-of-function mutant stocks used in this study were the deficiencies *Df(3R)Antp17 (tub<sup>def</sup>*; removing both *atub84B* and *atub84D*; Duncan & Kaufman, 1975, Jenkins, Saunders et al., 2017), *Df(2L)Exel6015 (sta<sup>Df</sup>*; Duncan, Lytle et al., 2013), *Df(3L)BSC553 (clasp<sup>Df</sup>*; Bloomington stock #25116; Beaven, Dzhindzhev et al., 2015), *Df(3R)tauMR22 (tau<sup>Df</sup>*; Doerflinger, Benton et al., 2003) and the loss-of-function mutant alleles *α-tub84B<sup>KO</sup>* (an engineered null-allele; Jenkins et al., 2017), *chromosome bows<sup>2</sup> (clasp<sup>2</sup>*, an amorph allele; Inoue, do Carmo Avides et al., 2000), *Eb1<sup>04524</sup>*, *Eb1<sup>5</sup>* (strong loss-of-function mutant alleles; Elliott, Cullen et al., 2005), *futsch<sup>P158</sup> (MAP1B*; a deficiency uncovering the *futsch* locus; Hummel, Krukkert et al., 2000), *msps<sup>A</sup>* (a small deletion causing a premature stop after 370 amino acids; gift from H. Ohkura, unpublished), *msps<sup>146</sup>* (Brittle & Ohkura, 2005), *sentin<sup>AB</sup> (short spindle2<sup>AB</sup>*, *ssp2<sup>AB</sup>*; Gluszek, Cullen et al., 2015), *tacc<sup>1</sup> (dTACC<sup>1</sup>*; Gergely, Kidd et al., 2000), *shot<sup>3</sup>* (the strongest available allele of *short stop*; Kolodziej, Jan et al., 1995, Sánchez-Soriano, Travis et al., 2009), *sta<sup>KO</sup>* (Yang, Inaki et al., 2012), *tau<sup>KO</sup>* (a null allele; Burnouf, Gronke et al., 2016). Gal4 driver lines used were *elav-Gal4* (1<sup>st</sup> and 3<sup>rd</sup> chromosomal, both expressing pan-neuronally at all stages; (Luo, Liao et al., 1994), *GMR31F10-Gal4* (Bloomington #49685; expressing in T1 medulla neurons; (Qu, Hahn et al., 2019). Lines for targeted gene expression were *UAS-Eb1-GFP* and *UAS-shot-Ctail-GFP* (Alves-Silva, Sánchez-Soriano et al., 2012), *UAS-shot<sup>ABD</sup>-GFP* (Qu, 2015), *UAS-shot<sup>3MTLS</sup>-GFP* (Alves-Silva et al., 2012), *UAS-dtau-GFP* (Doerflinger et al., 2003), *UAS-GFP-α-tubulin84B* (Grieder, de Cuevas et al., 2000) and further lines generated here (see below).

### Drosophila primary cell culture

*Drosophila* primary neuron cultures were done as described previously (Prokop, Küppers-Munther et al., 2012, Qu, Hahn et al., 2017). Stage 11 embryos were treated for 90 s with bleach to remove the chorion, sterilized for ~30 s in 70% ethanol, washed in sterile Schneider's medium containing 20% fetal calf serum (Schneider's/FCS; Gibco), and eventually homogenized with micro-pestles in 1.5 centrifuge tubes containing 21 embryos per 100 µl dispersion medium (Prokop et al., 2012) and left to incubated for 4 min at 37°C. Dispersion was stopped with 200 µl Schneider's/FCS, cells were spun down for 4 mins at 650 g, supernatant was removed and cells re-suspended in 90 µl of Schneider's/FCS, and 30 µl drops were placed in culture chambers and covered with cover slips. Cells were allowed to adhere to cover slips for 90-120

min either directly on glass or on cover slips coated with a 5 µg/ml solution of concanavalin A, and then grown as a hanging drop culture at 26°C as indicated.

To eliminate a potential maternal rescue of mutants (i.e. reduction of the mutant phenotype due to normal gene product deposition from the wildtype gene copy of the heterozygous mothers in oocytes (Prokop, 2013), we used a pre-culture strategy (Prokop et al., 2012, Sánchez-Soriano, Gonçalves-Pimentel et al., 2010) where cells were incubated in a tube for 7 days before they were plated on coverslips.

For cultures from larval brains, L3 brains (2-3 per cover slip) were dissected in PBS, transferred into Schneider's/FCS medium, washed three times with medium and then proceed with homogenisation and dispersion as explained above

Transfection of *Drosophila* primary neurons was executed as described previously (Qu et al., 2019). In brief, 70-75 embryos per 100 µl dispersion medium were used. After the washing step and centrifugation, cells were re-suspended in 100 µl transfection medium [final media containing 0.1-0.5 µg DNA and 2 µl Lipofecatmine 2000 (L2000, Invitrogen), incubation following manufacturer's protocols (Thermo Fisher, Invitrogen) and kept for 24 hrs at 26°C. Cells were then treated again with dispersion medium, re-suspended in culture medium and plated out as described above.

#### Xenopus primary neuron experiments

Xenopus primary neuron cultures were obtained from embryonic neural tube. Eggs collected from female *X. laevis* frogs were fertilised in vitro, dejellied and cultured following standard methods (Sive, Grainger et al., 2010). Embryos were grown to stage 22–24 (Nieuwkoop & J., 1994), and neural tubes were dissected as described (Lowery, Faris et al., 2012). Three neural tubes were transferred to an Eppendorf tube containing 150 µl CMF-MMR (0.1 M NaCl, 2.0 mM KCl, 1.0 mM EDTA, 5.0 mM HEPES, pH 7.4), 10 min later centrifuged at 1000 g for 5 min, and 150 µl of Steinberg's solution (58 mM NaCl, 0.67 mM KCl, 0.44 mM Ca(NO<sub>3</sub>)<sub>2</sub>, 1.3 mM MgSO<sub>4</sub>, 4.6 mM Tris, pH 7.8) was added to the supernatant to follow with the tissue dissociation using a fire polished glass Pasteur pipet. Cells were seeded in 100 µg/ml Poly-L-lysine and 10 µg/ml laminin pre-treated 60mm plates, and after 2 hr the media was replaced by plating culture media (50% Ringer's, 49% L-15 media, 1% Fetal Bovine Serum, 25 ng/µl NT3 and BDNF, plus 50 µg/ml penicillin/streptomycin and gentamycin, pH 7.4 and filter sterilized) and kept for 24 hr before imaging.

All experiments were approved by the Boston College Institutional Animal Care and Use Committee and performed according to national regulatory standards.

The embryos were injected four times in dorsal blastomeres at two-to-four cell stage with 6 ng of the validated XMAP215 morpholino (MO; Lowery, Stout et al., 2013), 10 ng of the validated Tau MO (Liu, Wang et al., 2015), and/or 5 ng of a newly designed splice site MO for EB3 (3'CTCCCAATTGTACCTACTTTGTG5'; for verification see Fig3-S1), in order to obtain a 50% knockdown of each.

To assess EB1 comet dynamics and comet amounts, 300 pg of MACF43-Ctail::GFP, an Eb protein-binding 43-residue fragment derived from the C-terminal regions of hMACF2 (human microtubule actin crosslinking factor 2; Fig.3F-F'''; Honnappa, Gouveia et al., 2009, Slater, Cammarata et al., 2019), was co-injected with the MO.

#### Immunohistochemistry

Primary fly neurons were fixed in 4% paraformaldehyde (PFA; in 0.05 M phosphate buffer, pH 7–7.2) for 30 min at room temperature (RT). For anti-Eb1 and anti-GTP-tubulin staining, cells were fixed for 10 mins at -20°C in +TIP fix (90% methanol, 3% formaldehyde, 5 mM sodium carbonate, pH 9; stored at -80°C and added to the cells) (Rogers, Rogers et al., 2002), then washed in PBT (PBS with 0.3% TritonX). Antibody staining and washes were performed with PBT. Staining reagents: anti-tubulin (clone DM1A, mouse, 1:1000, Sigma; alternatively, clone YL1/2, rat, 1:500, Millipore Bioscience Research Reagents); anti-DmEb1 (gift from H. Ohkura; rabbit, 1:2000; Elliott et al., 2005); anti-GTP-tubulin (hMB11; human, 1:200; AdipoGen; Dimitrov, Quesnoit et al., 2008); anti-Shot (1:200, guinea pig; Strumpf & Volk, 1998); anti-Elav (Elav-7E8A10; rat, 1:1000; Developmental Studies Hybridoma Bank, The University of Iowa, IA, USA; O'Neill, Rebay et al., 1994); anti-GFP (ab290, Abcam, 1:500); Cy3-conjugated anti-HRP (goat, 1:100, Jackson ImmunoResearch); F-actin was stained with phalloidin conjugated with TRITC/Alexa647, FITC or Atto647N (1:100 or 1:500; Invitrogen and Sigma). Specimens were embedded in ProLong Gold Antifade Mountant (ThermoFisher Scientific).

### Western blot analysis of *Xenopus* embryos

For protein extraction, 10 embryos were transferred to a centrifuge tube with 800 µl lysis buffer (50 mM Tris pH 7.5, 5% glycerol, 0.2% IGEPAL/NP-40, 1 mM EDTA, 1.5 mM MgCl<sub>2</sub>, 125 mM NaCl, 25 mM NaF, 1 mM Na<sub>3</sub>VO<sub>4</sub>), homogenised with a sterile pestle and, after 10 min, centrifuged at 13000 rpm for 15-20 min. The supernatant was collected and the protein concentration determined with the Micro BCA™ Protein Assay Kit (Thermo Fisher Scientific). 80 µg protein were loaded into a 10 % SDS gel and stained with anti-Tau (clone Tau46, T9450, mouse, 1:1000, Sigma-Aldrich).

### Dissection of adult heads

For *in vivo* studies, brain dissections were performed in Dulbecco's PBS (Sigma, RNB2227) after briefly sedating them on ice. Dissected brains with their laminas and eyes attached were placed into a drop of Dulbecco's PBS on MatTek glass bottom dishes (P35G1.5-14C), covered by coverslips and immediately imaged with a 3i Marianas Spinning Disk Confocal Microscope.

### Microscopy and data analysis

Standard imaging was performed with AxioCam 506 monochrome (Carl Zeiss Ltd.) or MatrixVision mvBlueFox3-M2 2124G digital cameras mounted on BX50WI or BX51 Olympus compound fluorescent microscopes. For the analysis of *Drosophila* and *Xenopus* primary neurons, we used the following parameters:

Axon length was measured from cell body to growth cone tip using the segmented line tool of ImageJ (Alves-Silva et al., 2012, Sánchez-Soriano et al., 2010).

Degree of MT disorganisation in axons was measured as "MT disorganisation index" (MDI) described previously (Qu et al., 2019, Qu et al., 2017); in short: the area of disorganisation was measured with the freehand selection in ImageJ; this value was then divided by axon length (see above) multiplied by 0.5 µm (typical axon diameter, thus approximating the expected area of the axon if it were not disorganised).

Eb1 comet amounts were approximated by using product of comet mean intensity and length. For this, a line was drawn through each comet (using the segmented line tool in FIJI) and length

as well as mean staining intensity (of Eb1 or GTP-tub in fixed *Drosophila* and MACF43::GFP in a movie still in *Xenopus* neurons) was determined.

To measure MT disorganisation in the optic lobe of adult flies, *GMR31F10-Gal4* (Bloomington #49685) was used to express *UAS- $\alpha$ -tubulin84B-GFP* (Grieder et al., 2000) in a subset of lamina axons which projects within well-ordered medulla columns (Prokop & Meinertzhagen, 2006). Flies were left to age for 26-27 days (about half their life expectancy) and then their brains were dissected out, mounted in Mattek dishes and imaged using a 3i spinning disk confocal system at the ITM Biomedecial imaging facility at the University of Liverpool. A section of the medulla columns comprising the 4 most proximal axonal terminals was used to quantify the number of swellings and regions with disorganised MTs.

To measure MT polymerisation dynamics, movies were collected on an Andor Dragonfly200 spinning disk upright confocal microscope (with a Leica DM6 FS microscope frame) and using a 100x/1.40 UPlan SAPO (Oil) objective. Samples were excited using 488nm (100%) and 561nm (100%) diode lasers via Leica GFP and RFP filters respectively. Images were collected using a Zyla 4.2 Plus sCMOS camera with a camera gain of 1x. The incubation temperature was set to 26°C. Time lapse movies were constructed from images taken every 1 s for 1 mins. To measure comet velocity and lifetime, a line was drawn that followed the axon using the segmented line tool in ImageJ. A kymograph was then constructed from average intensity in FIJI using the KymoResliceWide macro (Cell Biology group, Utrecht University) and events scored via the Velocity Measurement Tool Macro (Volker Baecker, INSERM, Montpellier, RIO Imaging; J. Rietdorf, FMI Basel; A. Seitz, EMBL Heidelberg). For each condition at least 15 cells were analysed in  $\geq 2$  independent repeats.

Time lapse imaging for *Xenopus* primary cultures was performed with a CSU-X1M 5000 spinning-disk confocal (Yokogawa, Tokyo, Japan) on a Zeiss Axio Observer inverted motorized microscope with a Zeiss 63x Plan Apo 1.4 numerical aperture lens (Zeiss, Thornwood, NY). Images were acquired with an ORCA R2 charge-coupled device camera (Hamamatsu, Hamamatsu, Japan) controlled with Zen software. Time lapse movies were constructed from images taken every 2 s for 1 min. The MACF43 comets' velocities and lifetime were analysed with plusTipTracker software. The same parameters were used for all movies: maximum gap length, eight frames; minimum track length, three frames; search radius range, 5–12 pixels; maximum forward angle, 50°; maximum backward angle, 10°; maximum shrinkage factor, 0.8; fluctuation radius, 2.5 pixels; and time interval 2 s.

Images were derived from at least 2 independent experimental repeats performed on different days, for each of which at least 3 independent culture wells were analysed by taking a minimum of 20 images per slide. For statistical analyses, Kruskal–Wallis one-way ANOVA with *post hoc* Dunn's test or Mann–Whitney Rank Sum Tests (indicated as  $P_{MW}$ ) were used to compare groups,  $r$  and  $p$ -value for correlation were determined via non-parametric Spearman correlation analysis. All raw data of our analyses are provided as supplementary Excel files T1-6.

## Molecular biology

To generate the *UAS-msps<sup>FL</sup>-GFP* (aa1-2050) and *UAS-msps <sup>$\Delta$ Cterm</sup>* (aa1-1322) constructs, eGFP was PCR-amplified from pcDNA3-EGFP and *msps* sequences from cDNA clone *LP04448* (DGRC; FBcl0189229) using the following primers:

<i>msps<sup>FL</sup></i>	and	<i>msps<sup><math>\Delta</math>Cterm</sup></i>	fw:
GAATAGGGAATTGGGAATTCGTTAGGCGCGCCAACATGGCCGAGGACACAGAGTAC			



*msps*<sup>FL</sup> rev:  
CAAGAAAGAGAATCATGCCCAAGGGCCCGGTAGCGGCAGCGGTAGCGTGAGCAAGGGC  
GAG

*msps*<sup>ΔCterm</sup> rev:  
GATGGAGGGTCTAAAATCGCATATGGGTAGCGGCAGCGGTAGCGTGAGCAAGGGCGAG  
GAG

*eGFP* fw:  
GAGAATCATGCCCAAGGGCCCGGTAGCGGCAGCGGTAGCGTGAGCAAGGGCGAGGAG  
CTG

*eGFP* rev:  
CTCTCGGCATGGACGAGCTGTACAAGTAGGCGGCCCGCTCGAGGGTACCTCTAGAG

The *msps* and *eGFP* sequences were introduced into *pUAST-attB* via Gibson assembly (ThermoFisher) using *EcoRI* and *XhoI*. To generate transgenic fly lines, *pUAST-attB* constructs were integrated into *PBac{yellow[+]-attP-9A}VK00024* (Bloomington line #9742) via PhiC31-mediated recombination (outsourced to Bestgene Inc).

## Results

### Eb1, Msps/XMAP215 and Tau share the same combination of loss-of-function phenotypes in axons

Many candidate regulators have been proposed to regulate MT polymerisation in axons, comprising factors that are MT plus end-associating, MT shaft-binding or involved in tubulin provision (Voelzmann et al., 2016). To reveal the core regulatory machinery necessary for axonal MT polymerisation, we performed a detailed loss-of-function study with a set of candidate factors using MT polymerisation dynamics and axon length as readouts. Of the pool of MT plus end-associating factors, we included Eb1, Shot, CLASP/Chb (Chromosome bows) and the XMAP215 homologue Msps; as MT shaft-binding candidates, we chose Tau and Map1b/Futsch; to explore the impact of tubulin availability on polymerisation, we used α1-tubulin/αtub84B, the predominant α-tubulin expressed in the fly nervous system (FlyAtlas 2, University of Glasgow, UK; A.V., unpublished) and the tubulin regulator Stathmin (see Discussion for more details on these factors).

To study these candidates, we analysed embryo-derived primary neurons carrying loss-of-function mutations for the respective genes. To exclude that phenotypes are masked by maternal contribution (i.e. healthy gene product deposited in the eggs by the heterozygous mothers), we used additional strategies (Prokop et al., 2012, Sánchez-Soriano et al., 2010): either we analysed late larval brain-derived primary neurons at 18 HIV (from now on referred to as larval neurons); if mutants did not reach larval stages, we used embryo-derived neurons that were kept for 5-7 days in pre-culture to deplete maternal product and then plated and grown for 12 hrs (pre-cultured neurons). In all cases, primary neurons were immuno-stained either for endogenous tubulin to assess axon length, or for endogenous Eb1 protein to gain a first insight into the polymerisation state of axonal MTs.

Eb1 staining revealed that loss of all factors, except Shot and Futsch, displayed a significant reduction in the number of plus end comets (Figs. 1A-D, I and 1-S1A). In addition, we measured the mean intensities and mean lengths of Eb1 comets and used the product of these two



parameters to approximate Eb1 amounts at MT plus ends. The strong hypomorphic *Eb1*<sup>04524</sup> mutant allele is known to display severe, but not complete reduction of protein levels (Elliott et al., 2005); accordingly, Eb1 amounts at MT plus ends were severely, but not completely diminished in neurons mutant for this allele (Figs. 1D,J and 1-S1B). Out of the remaining seven candidate factors, only two further genes showed the same qualitative mutant phenotype: *msps*<sup>A/A</sup> showed a reduction almost as strong as *Eb1*<sup>04524</sup>, and *tau*<sup>KO/KO</sup> mutant neurons showed a milder but reliable Eb1 depletion (Fig. 1B,C, J). In all cases, the drop in Eb1 amounts was to almost equal parts due to reductions in comet length and in intensity (Fig. 1-S2A,B) and, across all genotypes tested, they correlated well with reduced comet velocities and lifetimes when assessed in live imaging experiments (using the C-terminal Shot domain Shot-Ctail::GFP as readout for plus end dynamics; Fig. 1K,L and 1-S2C-E). Our data demonstrate therefore that similar comet length/velocity correlations made in *in vitro* (Roostalu, Thomas et al., 2020) are relevant in cellular contexts.

To assess whether observed reductions in the number or dynamics of MT plus end comets correlate with impaired axon growth, we performed tubulin staining and measured axon length. Out of the eight factors, all but Futsch/MAP1B showed a decrease in axon length ranging between 10 and 43% when compared to parallel control cultures with wild-type neurons (Figs. 1E-H, M and 1-S1C). In these experiments, a fraction of genotypes showed prominent MT bundle disintegration where MTs are disorganised and display intertwined, criss-crossing curls (white arrowheads in Fig. 1F-H). When quantifying these phenotypes using the MT disorganisation index (MDI; see methods), four of eight candidates showed significant MT disorganisation including loss of Tau, Msps, Shot and Eb1 (Figs. 1F-H,N and 1-S1D), of which the latter two confirm previous reports (Alves-Silva et al., 2012).

Therefore, out of eight candidate factors assessed with four phenotypic readouts (drop in comet numbers, reduced Eb1 amounts/dynamics, shorter axons, MT disorganisation), Futsch deficiency was the only condition showing no obvious defects. In contrast, loss of Eb1, Msps and Tau stood out by displaying all four phenotypes, of which Tau consistently has a milder effect. We therefore aimed to understand why these three factors share such a characteristic combination of phenotypes.

### Neuronal Eb1, Msps and Tau are functionally linked and required *in vivo*

Next we assessed whether Eb1, Msps and Tau are functionally related. For this, we performed genetic interaction studies where heterozygous conditions (i.e. one mutant and one normal copy) of genes are used to reduce their respective protein levels: if reduced protein levels of different genes combined in the same neurons cause a phenotype, this suggests that they function in a common pathway. For our studies, we used larval neurons and five different readouts: axon length (Fig. 2A), MT disorganisation (Fig. 2A'), Eb1 amounts at MT plus ends (Fig. 2A''), comet numbers (Fig. 2-S1A) and comet dynamics (Fig. 2-S1B).

To assess the baseline, we analysed single-heterozygous mutant neurons (*Eb1*<sup>04524/+</sup>, *msps*<sup>A/+</sup> or *tau*<sup>KO/+</sup>), none of which displayed any phenotypes (Figs. 2A-A'' and 2-S1A,B). However, when bringing heterozygous conditions of these genes together in the same neurons, certain genetic combinations displayed significant phenotypes (Fig. 2A'-A'' and 2-S1A,B): *Eb1*<sup>04524/+</sup> *msps*<sup>A/+</sup> and *tau*<sup>KO/+</sup> *msps*<sup>A/+</sup> double-heterozygous neurons displayed only a mild but significant reduction in Eb1 amounts at MT plus ends and a trend towards stronger MT disorganisation; the phenotypes were further enhanced for all five readouts in *Eb1*<sup>04524/+</sup> *msps*<sup>A/+</sup> *tau*<sup>KO/+</sup> triple-heterozygous neurons. These data suggest that the three factors are functionally linked when

regulating MT plus ends, axon growth and MT organisation.

The triple-heterozygous condition had a similar effect in fly brains *in vivo*. We could show this using the T1 subset of medulla neurons in the adult optic lobe which contain prominent axonal MTs, arranged into tight bundles that can be visualised with  $\alpha$ -tubulin::GFP labelling (Qu et al., 2019). We found that the axons of T1 medulla neurons from triple-heterozygous mutant adult flies show a strong increase in areas of MT bundle disorganisation compared to controls, with MTs becoming unbundled and twisted and axons displaying prominent swellings (Fig.3A-D). These data strongly suggest that the functional network of Eb1, Msps and Tau is relevant *in vivo*.

### The functional unit of Eb1, Msps and Tau is evolutionarily conserved in *Xenopus* neurons

In order to evaluate whether the functional network of Eb1, Msps and Tau might be conserved evolutionarily, we used frog primary neurons. In the frog *Xenopus laevis*, there is only one *tau* gene (*mapt/microtubule associated protein tau*), *XMAP215* is the only *msps* homologue (*ckap5/cytoskeleton associated protein 5*), and *EB3* (*mapre3/microtubule associated protein RP/EB family member 3*) is the only one of three *Eb1* homologues that is prominently expressed in the nervous system (Bowes, Snyder et al., 2009, Karimi, Fortriede et al., 2017). We used morpholinos against these three genes. Similar to our strategy in *Drosophila*, we analysed MTs by staining for endogenous tubulin (Fig.3E-E'''), and measured Eb3 comet amounts in live movies using the Eb protein-binding peptide MACF43-Ctail::GFP as readout (see Methods; Honnappa et al., 2009, Slater et al., 2019).

To approximate heterozygous mutant conditions used in our *Drosophila* experiments, we adjusted morpholino concentrations to levels that achieved knock-down of each of the three genes to ~50% (Fig. 3-S1A-B and (Lowery et al., 2013, Slater et al., 2019). Individual knock-downs to approximately 50% did not cause prominent decreases in MACF43::GFP comet amounts or increases in MT disorganisation; but when knock-down of all three factors was combined in the same neurons, we found a reduction in MACF43::GFP comet amounts to 60% and a 4.8 fold increase in MT disorganisation (Figs. 3E''',F''',G,H and 3-S1C,D).

Together, these results suggest that there is functional interaction between the three genes also in *Xenopus*, and that their operation as a functional unit is evolutionarily conserved. This raises the question as to what mechanisms can explain the joined function of these proteins.

### Eb1, Msps and Tau operate as one functional unit with key roles played by Eb1

We next asked whether the three factors are hierarchically and/or interdependently organised into a functional unit, or whether they regulate the assessed MT properties through independent parallel mechanisms. To distinguish between these possibilities (Avery & Wasserman, 1992), we combined homozygous mutant conditions of the three mutant alleles in the same neurons (*Eb1*<sup>04524/04524</sup> *msps*<sup>A/A</sup> *tau*<sup>KO/KO</sup>) and asked whether this condition enhances phenotypes over single-homozygous conditions (indicating parallel mechanisms), or whether they show no further increases (reflecting a functional unit).

Since the combined triple-homozygous condition does not survive into the late larval stage, we used embryonic pre-cultured neurons for these experiments. As reference we used *Eb1*<sup>04524/04524</sup>, *msps*<sup>A/A</sup> and *tau*<sup>KO/KO</sup> single mutant neurons; since *Eb1*<sup>04524</sup> is a strong but not a total loss-of-function allele (Elliott et al., 2005), we added neurons homozygous for

*Df(2R)Exel6050 (Eb1<sup>Df</sup>)*, a deficiency uncovering the entire *Eb1* locus (see Methods). Of the four conditions, *Eb1<sup>Df/Df</sup>* neurons showed the strongest phenotypes, thus setting the reference bar for the triple-homozygous mutant neurons; we found that having the mutations combined did not enhance the phenotypes beyond that of *Eb1<sup>Df</sup>* (Fig. 2B-B”).

These results are consistent with a model where the three proteins act as a functional unit. Within this unit, the three factors show the same qualitative loss-of-function phenotypes. However, there is a clear order of severity with *Eb1<sup>Df/Df</sup>* > *msps<sup>1/1</sup>* > *tau<sup>KO/KO</sup>* across all phenotypes assessed (Figs.2, 2-S1; see Discussion), suggesting that Eb1 is of particular importance within the functional unit. This is also highlighted when plotting Eb1 amounts against MT disorganisation from a range of different genetic conditions analysed throughout this study (Fig.2-S2A). This plot revealed that there is a highly significant inverse correlation between Eb1 comet amounts and MT disorganisation (Figs. 2C and 2-S2), suggesting that Eb1 is the key factor within the functional unit that mediates to MT bundle promotion.

### Eb1 and Msps depend on each other for MT plus end localisation

To understand the functional unit, we next focussed on the mechanistic links between Msps and Eb1. First we started with co-localisation studies by co-expressing Msps::GFP together with Eb1::RFP in *Drosophila* embryonic primary neurons. In these experiments, both proteins prominently localised at the same MT plus ends, with Msps::GFP localising slightly distal to Eb1 (Fig. 4A-A”, Movie M1), as was similarly reported *in vitro* (Maurer, Cade et al., 2014). Their localisation at the same MT plus ends was even clearer in kymographs of live movies where both proteins remained closely associated during comet dynamics (Fig.4B,B’).

In previous sections we reported that loss of Msps causes severe Eb1 depletion at MT plus ends (Fig1. 1B, D and 1-S1B), suggesting a requirement of Msps for Eb1's MT plus-end localisation. We hypothesised that the role of Msps as a tubulin polymerase (Brouhard et al., 2008) helps to sustain a prominent GTP-tubulin cap as important prerequisite for EB1 binding (Zanic et al., 2013). In support of this hypothesis, immunostaining for GTP-tubulin in *msps<sup>1</sup>* mutant neurons revealed length reductions of GTP caps that were as severe as the reduction observed for Eb1 comets (Figs. 1J vs. 5-S2C). This result together with our finding of reduced comet velocity in *msps<sup>1</sup>* mutant neurons (Fig. 1K) are consistent with our hypothesis that Msps-dependent polymerisation increases Eb1 amounts at MT plus ends (see Discussion).

Next we investigated whether Eb1 may influence Msps function. We expressed Msps::GFP in *Eb1<sup>04524</sup>* mutant neurons and found a severe depletion of Msps at growing MT ends when compared to controls (Fig. 4C, C’; Movies M2 and M3), suggesting that Msps is no longer efficiently recruited to the plus ends of polymerising MTs. Mechanistically, it was shown *in vitro* and other cell systems that Msps/XMAP215 can bind MT plus ends independently, but that Eb proteins can enhance its binding (Maurer et al., 2014, Zanic et al., 2013). Such enhanced Eb protein-dependent recruitment of Msps/XMAP215 can be mediated by adaptors such as SLAIN in vertebrates or TACC (Transforming acidic coiled-coil protein) or Sentin in non-neuronal *Drosophila* cells (Brouhard et al., 2008, Lee, Gergely et al., 2001, Li, Miki et al., 2011, Li et al., 2012, Lowery et al., 2013, Tang, Rui et al., 2020, van der Vaart, Franker et al., 2012). To test potential roles of candidate adaptors in fly neurons, we performed functional studies with *tacc<sup>1</sup>* and *sentin<sup>ΔB</sup>* loss-of-function mutant alleles. We found that primary neurons carrying these mutant alleles failed to display axon shortening or MT disorganisation, thus arguing against a prominent role of these factors to Eb1-dependent Msps recruitment (details in Fig.4-S1A,B). As

a complementary approach, we generated a *msps*<sup>ΔCterm</sup>-GFP construct which lacks the C-terminal domain essential for the interaction with adaptors (Fig.4D; Fox, Howard et al., 2014, Mortuza, Cavazza et al., 2014). When *msps*<sup>ΔCterm</sup>-GFP or *msps*<sup>FL</sup>-GFP length controls were transfected into *msps*<sup>A/146</sup> mutant neurons, we found that both protein variants were similarly able to improve axon length and MT disorganisation defects, further arguing against the requirement of adaptors (Fig.4D,D') in fly neurons.

In conclusion, our data suggest a scenario where Eb1 and Msps require each other to achieve prominent MT plus-end localisation. Msps likely maintains Eb1 at MT plus ends through promoting GTP-cap formation. *Vice versa*, Eb1 facilitates Msps recruitment through a mechanism that might involve structural maturation of MT plus ends (see Discussion; Maurer et al., 2014, Zanic et al., 2013).

### Tau promotes Eb1 pools at MT plus ends by outcompeting it from lattice binding

Similar to Msps, we found that also loss of Tau leads to a reduction of Eb1 comet sizes in both *Drosophila* (Fig.1C,J and 1-S2A,B) and *Xenopus* neurons (Fig.3-S1G-I). Immuno-histochemical studies of wild-type fly neurons revealed Tau localisation along MT lattices which does not extend into the Eb1 comet at the MT plus end (Fig.5A'A"). This distribution is consistent with reports that Tau has a higher affinity for GDP-tubulin (Castle, McKibben et al., 2020, Duan, Jonasson et al., 2017) and does suggest that Tau promotes Eb1 plus end localisation through an indirect mechanisms which does not involve co-localisation.

We noticed that the reduction of Eb1 comet sizes in Tau-deficient neurons is accompanied by a 20% increase in the intensity of Eb1 all along MT lattices (Fig.5C,E for 6 day pre-culture, Fig.5-S2A for 6HIV). This effect is specific to *tau* and not observed in *msps*<sup>A/A</sup> mutant neurons (Fig. 5-S2A,B). Tau has previously been shown to protect MTs against Katanin-induced damage (Qiang, Yu et al., 2006). Therefore, we reasoned that the increase of Eb1 on MT lattices upon loss of Tau could be a consequence of MT repair mechanisms leading to an increase in GTP-tubulin along the lattice which could recruit Eb1 (Vemu, Szczesna et al., 2018). However, in spite of increased Eb1 binding, MT lattices in Tau-deficient neurons did not show obvious increases in GTP-tubulin (Fig. 5-S1B, D), arguing against the repair hypothesis. In the same specimens, GTP-tubulin amounts at MT plus ends were clearly reduced, thus mirroring Eb1 comet depletion in Tau deficient neurons (Figs. 1J vs. 5-S1A-C) and suggesting that GTP-tubulin staining is sufficiently sensitive to make quantitative statements in our model.

We next hypothesised that Tau may competitively prevent Eb1 from binding the MT lattice, as similarly observed for other MAPs (Qiang, Sun et al., 2018). In support of this notion, we found that low levels of Eb1 localisation along MT lattices observed in wild-type neurons are further decreased when Tau is over-expressed (Fig. 5-S1E). A similar phenomenon has been observed *in vitro* with mammalian versions of the two proteins (Ramirez-Rios, Denarier et al., 2016) suggesting that this mechanism is evolutionarily conserved.

We reasoned therefore that MT lattices may turn into a sink for Eb1 if Tau is absent. Given the high density of MTs in the narrow axons, this aberrant binding could sequester Eb1 pools away from MT plus ends. To test this possibility, we expressed Eb1::GFP in *tau*<sup>KO/KO</sup> mutant neurons and stained them with anti-Eb1 antibodies. In support of our hypothesis, these neurons showed a substantial further increase of Eb1 along MT lattices, but also replenished Eb1 amounts at MT plus ends (Fig. 5D-F). This treatment was sufficient to suppress Tau-deficient phenotypes, as reflected in the recovery of Eb1 comet dynamics (improved velocity and lifetime) and strongly



reduced MT disorganisation ('Eb1-GFP' in Fig. 5G-I). The latter finding further supports a role of Eb1 in promoting the bundled conformation of axonal MTs (Fig.2C, Fig.2-S2; see Discussion).

Specificity of this mechanism for Tau is demonstrated by parallel experiments expressing Eb1::GFP in *msps<sup>Δ/Δ</sup>* mutant neurons which failed to restore their MT plus end dynamics (Fig. 5-S2D,E). This result also provides further important information about the hierarchical relationships between Eb1, Msps and Tau within the functional unit (see Discussion). As a further control, we used Shot-Ctail::GFP (comparable to MACF43::GFP used in *Xenopus*; Figs. 3F and 6A), thus tracking MT plus ends without altering Eb1 levels. When expressing it in *tau<sup>KO/KO</sup>* mutant neurons, no rescue of MT plus end comet velocity and lifetime was observed ('Ctail-GFP' in Fig.5G,H).

In conclusion, we propose that Tau contributes to MT polymerisation dynamics and MT organisation in an indirect way through preventing that Eb1 is sequestered away from MT plus ends. This function of Tau might be particularly important in axons where relative MT densities are high (Prokop, 2020; see Discussion).

#### An Eb1- and spectraplakin-dependent guidance mechanisms explains roles of the functional unit in MT bundle organisation

As explained before, Eb1 amounts at MT plus ends inversely correlate with MT disorganisation (Figs.2C and 2-S2). Observed MT disorganisation in either Eb1-, Msps- or Tau-deficient neurons might therefore be a consequence of Eb1 loss from plus ends. We hypothesised that this phenomenon can be explained through a mechanism involving the *Drosophila* spectraplakin Shot. Shot has been proposed to link Eb1 at polymerising MT plus ends to cortical F-actin, in this way guiding the extension of MTs along the axonal surface into parallel bundles. Accordingly, depletion of either Shot or Eb1 causes MT disorganisation (Alves-Silva et al., 2012, Voelzmann, Liew et al., 2017; Fig.6F).

In support of this guidance hypothesis, we found that severe MT disorganisation observed in *Eb1<sup>1/+</sup> msp<sup>s</sup><sup>+/+</sup> tau<sup>+/+</sup>* triple-heterozygous mutant neurons (which have reduced Eb1 comet amounts; Fig.2A'') was significantly improved from 7.3-fold (with GFP-expression) to 1.4-fold when over-expressing full length Shot-FL::GFP (Fig.6B-C; both compared to wild-type controls).

To exclude that this rescue is mediated through different Shot-dependent mechanisms, in particular its role in MT stabilisation (Voelzmann et al., 2017), we repeated these experiments with Shot versions that maintain MT-stabilising activity but affect actin-Eb1 cross-linkage in two specific ways: (1) Shot<sup>ΔABD</sup>::GFP lacks the N-terminal calponin homology domain required for interaction with the actin cortex; (2) Shot<sup>3MTLS</sup>::GFP carries mutations in the C-terminal SxIP motifs required for the specific binding to Eb1 (Fig. 6A and F; see also Fig. 7A). Both Shot variants failed to rescue MT disorganisation in *Eb1<sup>04524/+</sup> msp<sup>s</sup><sup>1/+</sup> tau<sup>KO/+</sup>* triple-heterozygous mutant neurons (Fig.6B,C), consistent with a model where where Shot guides MTs downstream of Eb1 through cross-linking it to cortical F-actin. This conclusion is further supported by the finding that MT disorganisation observed in *Eb1<sup>04524/04524</sup>* mutant neurons is not further enhanced in *Eb1<sup>04524/04524</sup> shot<sup>3/3</sup>* double-mutant neurons (Figs. 6D, E).

We conclude that the polymerisation-promoting functional unit of Eb1, Msps and Tau appears to act through Shot-mediated MT guidance downstream of Eb1 to perform its function in axonal bundle organisation, as a key mechanism contributing to the formation and long-term maintenance of axons.



## Discussion

### New understanding of the role and regulation of MT polymerisation and guidance in axons

Understanding the machinery of MT polymerisation is of utmost importance in axons where MTs form loose bundles of enormous lengths which are essential for axonal morphogenesis and serve as life-sustaining transport highways (Prokop, 2020). They have to be maintained in functional state for up to a century in humans (Hahn et al., 2019). For this, MT polymerisation is required to generate new MTs, or to repair or replace them. The underpinning machinery is expected to be complex (Voelzmann et al., 2016), but its understanding will deliver new strategies for tackling developmental and degenerative axon pathologies.

Here we made important advances to this end. Having screened through 13 candidates (here and (Beaven et al., 2015), we found the three factors Eb1, Msps and Tau to stand out by expressing the same combination of phenotypes, and displaying strong functional interaction in *Drosophila* that is conserved in *Xenopus* neurons. We found that this machinery is not only important to maintain MT mass by driving polymerisation, but also for arranging MTs into bundles, thus highlighting MT polymerisation as a doubly important process for axon formation and maintenance.

Through carrying out this work in fly, we were able to demonstrate that the functional collaboration of the three factors is relevant *in vivo* and gain an understanding of the underlying mechanisms, both with respect to promoting MT polymerisation and their arrangement into parallel bundles (see details in Fig.7 and below).

Our mechanistic models are strongly supported by published data obtained through *in vitro* studies of MTs that match extremely well with virtually all our findings. Key examples are: (1) the complementary binding preferences of EB1 and Tau for GTP-/GDP-tubulin (Castle et al., 2020, Zanic, Stear et al., 2009); (2) the mutual enhancement of Eb1 and XMAP215/Msps originally suggested in *Xenopus* extracts and then demonstrated in reconstitution essays with purified proteins from fly and vertebrates (Kronja, Kruljac-Letunic et al., 2009, Li et al., 2012, Zanic et al., 2013); (3) the correlation of GTP cap size with comet velocity (Roostalu et al., 2020); (4) the reduction of comet numbers but not dynamics (Fig.1-S1) upon depletion of  $\alpha$ 1-tubulin or Stathmin (a prominent regulator of tubulin availability; Duncan et al., 2013, Manna, Grenningloh et al., 2007) which are consistent with *in vitro* observations that MT nucleation is far more sensitive to tubulin levels than polymerisation (Consolati, Locke et al., 2020). This list of similarities is in stark support of our model and a clear indication that many *in vitro* observation seem to apply in cellular contexts.

In the following we will discuss a mechanistic model (summarised in Fig.7) able to coherently integrate our experimental findings in neurons with current knowledge obtained from *in vitro* studies.

### Eb1 and XMAP215/Msps are core factors promoting MT polymerisation and guidance

At the core of this model lie Eb1 and XMap215/Msps. Of these, vertebrate XMAP215 and fly Msps are both known to be relevant for neuronal morphogenesis in fly and *Xenopus* (Lowery et al., 2013, Tang et al., 2020). Work in non-neuronal cells or *in vitro* have shown that Msps and XMAP215 both strongly enhance MT polymerisation, consistent with expected functions of this TOG-domain protein as a polymerase (Al-Bassam & Chang, 2011, Brouhard et al., 2008, Fox

et al., 2014, Howard & Hyman, 2009, Li et al., 2012, Zanic et al., 2013).

Eb1 is a known scaffold (Akhmanova & Steinmetz, 2015) and, accordingly, both *Drosophila* and vertebrate Eb1 seem to be only moderate promoters of MT polymerisation *in vitro* (Li et al., 2012, Ramirez-Rios et al., 2016, Zanic et al., 2013) and references within). Conserved binding partners of Eb proteins are the spectraplakins that can guide extending MT plus ends by cross-linking them to actin, relevant for MT guidance in axons and non-neuronal cells (Alves-Silva et al., 2012, Voelzmann et al., 2017, Wu, Kodama et al., 2008). Although spectraplakins might not be the only interactors involved in Eb1-dependent axonal MT guidance (Hahn et al., 2019), their contribution is prominent and our data clearly support this role of Shot (Fig.7E,E').

Taken together, it seems therefore reasonable to assume that, within the functional unit, Msps is the key promoter of polymerisation, and Eb1 the key mediator of MT guidance into bundles (Fig.7A,A'). However, to perform these functions, both factors have to be enriched in sufficient amounts at MT plus ends. For this, both proteins depend on each other: taking out Eb1 detaches not only Shot thus abolishing guidance, but also negatively impacts Msps localisation hence polymerisation (Fig.7B,B'); the same is true in reverse when removing Msps (Fig.7C,C') and may explain why loss of XMAP215 was reported to affect MT guidance in growth cones of frog neurons (Slater et al., 2019).

This mutual dependency is unlikely to involve their physical interaction, since MT plus end localisation of Eb1 is known to occur tens of nanometres behind XMAP215 (Maurer et al., 2014, Zanic et al., 2013). Furthermore, as detailed in the Results part, our data do not support an obvious role of adaptors in mediating Eb1- XMAP215 interactions (Figs.4D-D" and 4-S1). This deviates from other cellular contexts in which EB1 adaptors are required for Msps/XMAP215 MT plus end localisation (Lee et al., 2001, Li et al., 2011, Li et al., 2012, Nwagbara, Faris et al., 2014, Tang et al., 2020, van der Vaart et al., 2012), potentially reflecting context-specific variations in MT regulation; this has similarly been reported for the plus end-associating factor Clip170/190 which fails to form comets in axons of fly and mouse neurons (Beaven et al., 2015).

Instead, indirect mechanisms for mutual dependency of Eb1 and XMAP215/Msps were proposed in the context of *in vitro* studies: through promoting MT polymerisation, XMAP215 maintains a prominent GTP-cap thus enabling the binding of substantial amounts of Eb1 molecules (Maurer et al., 2014, Zanic et al., 2013). Restricted GTP-cap formation as a limiting factor for Eb1 binding would also explain why Eb1 over-expression fails to rescue Msps-deficient phenotypes (Fig.5-S2D-F). *Vice versa*, it was suggested that Eb1's ability to promote lateral protofilament contacts could assist in sheet formation at the very plus tip, thus facilitating the binding of XMAP215/Msps (Maurer et al., 2014, Zanic et al., 2013). We believe this mechanism to be the most likely to explain our findings.

#### Tau contributes through an indirect mechanism of competitive binding to MT lattices

Tau and Map1b/Futsch are known to promote MT polymerisation *in vitro* and axon growth in mouse and fly neurons through mechanisms that remain unclear (Brandt & Lee, 1993, Caceres & Kosik, 1990, Cleveland, Hwo et al., 1977, DiTella, Feiguin et al., 1996, Drechsel et al., 1992, Hummel et al., 2000, Kadavath, Hofele et al., 2015, Kiris, Ventimiglia et al., 2010, Levy, Leboeuf et al., 2005, Liu et al., 2015, Panda, Goode et al., 1995, Ramirez-Rios et al., 2016, Takei, Teng et al., 2000, Tymanskyj, Scales et al., 2012, Villarroel-Campos & Gonzalez-Billault, 2014).

In our cellular model, loss of Map1b/Futsch has no obvious effects, whereas Tau shares a surprising number of loss-of-function mutant phenotypes with those of Msps and Eb1. At least

one of these, loss of Eb proteins from MT plus ends, appears an evolutionarily well conserved phenomenon observed in fly neurons (Figs.1C,J), frog neurons (Fig.3-S1G-I), N1E-115 mouse neuroblastoma cells and primary mouse cortical neurons (Sayas, Tortosa et al., 2015). Sayas and co-workers originally reported also tau-mediated recruitment of Eb proteins to the MT lattice (analogous to MAP2-mediated Eb3 recruitment to MTs in dendrites; Kapitein, Yau et al., 2011). However, their subsequent *in vitro* work suggested that Tau outcompetes Eb1 at the lattice and Eb proteins outcompete Tau at MT plus ends (Ramirez-Rios et al., 2016), potentially involving sequestration through direct interaction in the cytoplasm - as would be consistent with other reports that Tau can bind Eb1 (Buey, Mohan et al., 2011, Duan et al., 2017).

We do not argue against such interaction and that it can potentially contribute to Eb protein loss from MT plus ends when tau is over-expressed (Ramirez-Rios et al., 2016); but it cannot explain why Eb1 comets are reduced when Tau is absent. Instead, the mechanism we propose is based on the known complementary binding preferences of Eb1 and Tau for GTP-/GDP-tubulin (Castle et al., 2020, Duan et al., 2017, Zanic et al., 2009). Thus, we find that Tau binds preferentially along MT shafts but not at plus ends, whereas Eb1 binds in complementary fashion and displays elevated shaft binding when Tau is absent (Fig.5C and 7D'). Such competitive binding behaviour is reminiscent of Tau's role in preventing MAP6 from binding in certain regions of the MT lattice (Baas & Qiang, 2019, Qiang et al., 2018); it is in agreement with the idea of a MAP code where similar MAP competition is assumed to regulate region-specific axonal transport (Monroy, Tan et al., 2020).

Given the high density of MTs in the narrow space of axons, we propose that lattice binding can generate a sink large enough to reduce Eb1 levels at MT plus ends, and our rescue experiments with Eb1::GFP overexpression strongly support this notion. In this way, loss of Tau generates a condition comparable to a modest Eb1 loss-of-function mutant phenotype, thus explaining why Tau shares its repertoire of loss-of-function phenotypes with Msps and Eb1 but with lower penetrance.

We propose that similar mechanisms might operate in smaller diameter axons in vertebrates, such as in parallel fibres of the cerebellum where Tau has demonstrated structural roles (Harada, Oguchi et al., 1994); they might explain the aforementioned findings of small Eb protein comets in cultured vertebrate neurons, as well as the reduction in MT numbers observed upon loss of Tau in *C. elegans* (Krieg, Stühmer et al., 2017). However, in larger diameter axons of vertebrates where MT densities are low (Prokop, 2020), the Eb1 depletion effect might be far less noticeable.

### Main conclusions and future perspectives

Here we have gained new understanding of MT polymerisation regulation in axons and have been able to propose a solid and consistent mechanistic model. This model aligns well with known *in vitro* data and our previous mechanistic models explaining Eb1/Shot-mediated MT guidance (Alves-Silva et al., 2012) and complementary functions of Shot and the cortical collapse factor Efa6 (Qu et al., 2019).

Developing such refined mechanistic models of increasing complexity is made possible through using one standardised *Drosophila* neuron system amenable to combinatorial genetic approaches - with enormous capacity to extend our understanding even further to other factors known to regulate MT polymerisation *in vitro* (Zanic et al., 2013). Gaining an understanding of the machinery regulating axonal MT polymerisation opens up new ways to investigate the

mechanisms behind other important observations, such as the finding that cortical actin has a regulatory impact on MT polymerisation in axons (Qu et al., 2017).

As another example, we found that loss of either Eb1, XMAP215/Msps or Tau all caused a reduction in comet numbers, potentially reflecting changes in MT nucleation activity, consistent with reports of nucleation-promoting roles of XMAP215 (Flor-Parra, Iglesias-Romero et al., 2018, Roostalu, Cade et al., 2015, Thawani, Kadzik et al., 2018, Wieczorek, Bechstedt et al., 2015). Extending work from MT polymerisation to nucleation is possible in the fly system and would have the potential to deliver explanations for how numbers of MTs can be regulated in reproducible, neuron-specific ways, thus addressing a fundamental aspect of axon morphology (Prokop, 2020).

By gradually assembling molecular mechanisms into regulatory networks that can explain axonal MT regulation at the cellular level, our studies come closer to explaining axonal pathologies which can then form the basis for the development of remedial strategies (Hahn et al., 2019).

## Acknowledgements

This work was made possible through support by the BBSRC to A.P (BB/I002448/1, BB/P020151/1, BB/L000717/1, BB/M007553/1) to N.S.S. (BB/M007456/1, BB/R018960/1), by the Leverhulme Trust to I.H. (ECF-2017-247), by the German Research Council (DFG) to A.V. (VO 2071/1-1), by NIH to L.A.L (R01 MH109651), and a postdoctoral fellowship from CONICYT to P.G.S. The Manchester Bioimaging Facility microscopes used in this study were purchased with grants from the BBSRC, The Wellcome Trust and The University of Manchester Strategic Fund. The Fly Facility has been supported by funds from The University of Manchester and the Wellcome Trust (087742/Z/08/Z). We thank Hiro Ohkura for kindly providing DmEb1 antibody and unpublished mutant alleles of *msps*. Stocks obtained from the Bloomington *Drosophila* Stock Center (NIH P40OD018537) were used in this study.

## References

- Adalbert R, Coleman MP (2012) Axon pathology in age-related neurodegenerative disorders. *Neuropathol Appl Neurobiol* 39: 90–108
- Aher A, Rai D, Schaedel L, Gaillard J, John K, Liu Q, Altelaar M, Blanchoin L, Thery M, Akhmanova A (2020) CLASP mediates microtubule repair by restricting lattice damage and regulating tubulin incorporation. *Current Biology*
- Akhmanova A, Steinmetz MO (2015) Control of microtubule organization and dynamics: two ends in the limelight. *Nat Rev Mol Cell Biol* 16: 711–726
- Al-Bassam J, Chang F (2011) Regulation of microtubule dynamics by TOG-domain proteins XMAP215/Dis1 and CLASP. *Trends Cell Biol* 21: 604–14
- Al-Bassam J, Kim H, Brouhard G, van Oijen A, Harrison SC, Chang F (2010) CLASP promotes microtubule rescue by recruiting tubulin dimers to the microtubule. *Dev Cell* 19: 245–58
- Alves-Silva J, Sánchez-Soriano N, Beaven R, Klein M, Parkin J, Millard T, Bellen H, Venken KJT, Ballestrem C, Kammerer RA, Prokop A (2012) Spectraplakins promote microtubule-mediated axonal growth by functioning as structural microtubule-associated proteins and EB1-dependent +TIPs (Tip Interacting Proteins). *J Neurosci* 32: 9143–58
- Avery L, Wasserman S (1992) Ordering gene function: the interpretation of epistasis in regulatory hierarchies. *Trends Genet* 8: 312–316



- 709 Baas PW, Qiang L (2019) Tau: it's not what you think. *Trends Cell Biol* 29: 452-461
- 710 Beaven R, Dzhindzhev NS, Qu Y, Hahn I, Dajas-Bailador F, Ohkura H, Prokop A (2015)
- 711 *Drosophila* CLIP-190 and mammalian CLIP-170 display reduced microtubule plus end
- 712 association in the nervous system. *Mol Biol Cell* 26: 1491-508
- 713 Bowes JB, Snyder KA, Segerdell E, Jarabek CJ, Azam K, Zorn AM, Vize PD (2009) Xenbase:
- 714 gene expression and improved integration. *Nucleic Acids Research* 38: D607-D612
- 715 Brandt R, Lee G (1993) The balance between tau protein's microtubule growth and nucleation
- 716 activities: implications for the formation of axonal microtubules. *J Neurochem* 61: 997-1005
- 717 Brittle AL, Ohkura H (2005) Mini spindles, the XMAP215 homologue, suppresses pausing of
- 718 interphase microtubules in *Drosophila*. *EMBO J* 24: 1387-96
- 719 Brouhard GJ, Stear JH, Noetzel TL, Al-Bassam J, Kinoshita K, Harrison SC, Howard J, Hyman
- 720 AA (2008) XMAP215 is a processive microtubule polymerase. *Cell* 132: 79-88
- 721 Buey RM, Mohan R, Leslie K, Walzthoeni T, Missimer JH, Menzel A, Bjelic S, Bargsten K,
- 722 Grigoriev I, Smal I, Meijering E, Aebersold R, Akhmanova A, Steinmetz MO (2011) Insights
- 723 into EB1 structure and the role of its C-terminal domain for discriminating microtubule tips
- 724 from the lattice. *Mol Biol Cell* 22: 2912-23
- 725 Burnouf S, Gronke S, Augustin H, Dols J, Gorsky MK, Werner J, Kerr F, Alic N, Martinez P,
- 726 Partridge L (2016) Deletion of endogenous Tau proteins is not detrimental in *Drosophila*. *Sci*
- 727 *Rep* 6: 23102
- 728 Caceres A, Kosik KS (1990) Inhibition of neurite polarity by tau antisense oligonucleotides in
- 729 primary cerebellar neurons. *Nature* 343: 461-3
- 730 Calkins DJ (2013) Age-Related Changes in the Visual Pathways: Blame It on the AxonAge-
- 731 Related Changes in the Visual Pathways. *Invest Ophthalmol Vis Sci* 54: ORSF 37-41
- 732 Castle BT, McKibben KM, Rhoades E, Odde DJ (2020) Tau avoids the GTP cap at growing
- 733 microtubule plus ends. *bioRxiv*: 2019.12.31.891234
- 734 Cleveland DW, Hwo SY, Kirschner MW (1977) Purification of tau, a microtubule-associated
- 735 protein that induces assembly of microtubules from purified tubulin. *J Mol Biol* 116: 207-25
- 736 Consolati T, Locke J, Roostalu J, Chen ZA, Gannon J, Asthana J, Lim WM, Martino F, Cvetkovic
- 737 MA, Rappsilber J, Costa A, Surrey T (2020) Microtubule Nucleation Properties of Single
- 738 Human  $\gamma$ TuRCs Explained by Their Cryo-EM Structure. *Developmental Cell* 53: 603-617.e8
- 739 Dimitrov A, Quesnoit MI, Moutel S, Cantaloube I, Po's C, Perez F (2008) Detection of GTP-
- 740 tubulin conformation *in vivo* reveals a role for GTP remnants in microtubule rescues. *Science*
- 741 322: 1353-1356
- 742 DiTella MC, Feiguin F, Carri N, Kosik KS, Caceres A (1996) MAP-1B/TAU functional
- 743 redundancy during laminin-enhanced axonal growth. *J Cell Sci* 109 ( Pt 2): 467-77
- 744 Doerflinger H, Benton R, Shulman JM, St Johnston D (2003) The role of PAR-1 in regulating
- 745 the polarised microtubule cytoskeleton in the *Drosophila* follicular epithelium. *Development*
- 746 130: 3965-75
- 747 Drechsel DN, Hyman AA, Cobb MH, Kirschner MW (1992) Modulation of the dynamic instability
- 748 of tubulin assembly by the microtubule-associated protein tau. *Mol Biol Cell* 3: 1141-54
- 749 Duan AR, Jonasson EM, Alberico EO, Li C, Scripture JP, Miller RA, Alber MS, Goodson HV
- 750 (2017) Interactions between tau and different conformations of tubulin: implications for tau
- 751 function and mechanism. *J Mol Biol* 429: 1424-1438
- 752 Duncan IW, Kaufman TC (1975) Cytogenic analysis of chromosome 3 in *Drosophila*
- 753 *melanogaster*: mapping of the proximal portion of the right arm. *Genetics* 80: 733-52
- 754 Duncan JE, Lytle NK, Zuniga A, Goldstein LS (2013) The microtubule regulatory protein
- 755 Stathmin is required to maintain the integrity of axonal microtubules in *Drosophila*. *PLoS One*
- 756 8: e68324



- 757 Elliott SL, Cullen CF, Wrobel N, Kernan MJ, Ohkura H (2005) EB1 is essential during *Drosophila*  
758 development and plays a crucial role in the integrity of chordotonal mechanosensory organs.  
759 *Mol Biol Cell* 16: 891-901
- 760 Flor-Parra I, Iglesias-Romero AB, Chang F (2018) The XMAP215 ortholog Alp14 promotes  
761 microtubule nucleation in fission yeast. *Curr Biol* 28: 1681-1691.e4
- 762 Fox JC, Howard AE, Currie JD, Rogers SL, Slep KC (2014) The XMAP215 family drives  
763 microtubule polymerization using a structurally diverse TOG array. *Mol Biol Cell* 25: 2375-92
- 764 Gasic I, Mitchison TJ (2019) Autoregulation and repair in microtubule homeostasis. *Curr Opin*  
765 *Cell Biol* 56: 80-87
- 766 Gergely F, Kidd D, Jeffers K, Wakefield JG, Raff JW (2000) D-TACC: a novel centrosomal  
767 protein required for normal spindle function in the early *Drosophila* embryo. *EMBO J* 19: 241-  
768 52
- 769 Gluszek AA, Cullen CF, Li W, Battaglia RA, Radford SJ, Costa MF, McKim KS, Goshima G,  
770 Ohkura H (2015) The microtubule catastrophe promoter Sentin delays stable kinetochore-  
771 microtubule attachment in oocytes. *J Cell Biol* 211: 1113-20
- 772 Grieder NC, de Cuevas M, Spradling AC (2000) The fusome organizes the microtubule network  
773 during oocyte differentiation in *Drosophila*. *Development* 127: 4253-4264
- 774 Hahn I, Voelzmann A, Liew Y-T, Costa-Gomes B, Prokop A (2019) The model of local axon  
775 homeostasis - explaining the role and regulation of microtubule bundles in axon maintenance  
776 and pathology *Neural Dev* 14: 10.1186/s13064-019-0134-0
- 777 Harada A, Oguchi K, Okabe S, Kuno J, Terada S, Ohshima T, Sato-Yoshitake R, Takei Y, Noda  
778 T, Hirokawa N (1994) Altered microtubule organization in small-calibre axons of mice lacking  
779 tau protein. *Nature* 369: 488-91
- 780 Honnappa S, Gouveia SM, Weisbrich A, Damberger FF, Bhavesh NS, Jawhari H, Grigoriev I,  
781 van Rijssel FJ, Buey RM, Lawera A, Jelesarov I, Winkler FK, Wuthrich K, Akhmanova A,  
782 Steinmetz MO (2009) An EB1-binding motif acts as a microtubule tip localization signal. *Cell*  
783 138: 366-76
- 784 Howard J, Hyman AA (2009) Growth, fluctuation and switching at microtubule plus ends. *Nat*  
785 *Rev Mol Cell Biol* 10: 569-74
- 786 Hummel T, Krukkert K, Roos J, Davis G, Klämbt C (2000) *Drosophila* Futsch/22C10 is a  
787 MAP1B-like protein required for dendritic and axonal development. *Neuron* 26: 357-370
- 788 Inoue YH, do Carmo Avides M, Shiraki M, Deak P, Yamaguchi M, Nishimoto Y, Matsukage A,  
789 Glover DM (2000) Orbit, a novel microtubule-associated protein essential for mitosis in  
790 *Drosophila melanogaster*. *J Cell Biol* 149: 153-66
- 791 Jenkins BV, Saunders HAJ, Record HL, Johnson-Schlitz DM, Wildonger J (2017) Effects of  
792 mutating alpha-tubulin lysine 40 on sensory dendrite development. *J Cell Sci* 130: 4120-4131
- 793 Kadavath H, Hofele RV, Biernat J, Kumar S, Tepper K, Urlaub H, Mandelkow E, Zweckstetter  
794 M (2015) Tau stabilizes microtubules by binding at the interface between tubulin  
795 heterodimers. *Proc Natl Acad Sci* 112: 7501-7506
- 796 Kapitein LC, Yau KW, Gouveia SM, van der Zwan WA, Wulf PS, Keijzer N, Demmers J,  
797 Jaworski J, Akhmanova A, Hoogenraad CC (2011) NMDA receptor activation suppresses  
798 microtubule growth and spine entry. *J Neurosci* 31: 8194-209
- 799 Karimi K, Fortriede JD, Lotay VS, Burns KA, Wang DZ, Fisher ME, Pells TJ, James-Zorn C,  
800 Wang Y, Ponferrada V G, Chu S, Chaturvedi P, Zorn AM, Vize PD (2017) Xenbase: a  
801 genomic, epigenomic and transcriptomic model organism database. *Nucleic Acids Res* 46:  
802 D861-D868
- 803 Kiris E, Ventimiglia D, Feinstein SC (2010) Quantitative analysis of MAP-mediated regulation of  
804 microtubule dynamic instability in vitro focus on Tau. *Methods Cell Biol* 95: 481-503
- 805 Kolodziej PA, Jan LY, Jan YN (1995) Mutations that affect the length, fasciculation, or ventral  
806 orientation of specific sensory axons in the *Drosophila* embryo. *Neuron* 15: 273-286

- Krieg M, Stühmer J, Cueva JG, Fetter R, Spilker K, Cremers D, Shen K, Dunn AR, Goodman MB (2017) Genetic defects in  $\beta$ -spectrin and tau sensitize *C. elegans* axons to movement-induced damage via torque-tension coupling. *Elife* 6: e20172
- Kronja I, Kruljac-Letunic A, Caudron-Herger M, Bieling P, Karsenti E (2009) XMAP215-EB1 interaction is required for proper spindle assembly and chromosome segregation in *Xenopus* egg extract. *Mol Biol Cell* 20: 2684-96
- Lee MJ, Gergely F, Jeffers K, Peak-Chew SY, Raff JW (2001) Msps/XMAP215 interacts with the centrosomal protein D-TACC to regulate microtubule behaviour. *Nat Cell Biol* 3: 643-9
- Levy SF, Leboeuf AC, Massie MR, Jordan MA, Wilson L, Feinstein SC (2005) Three- and four-repeat tau regulate the dynamic instability of two distinct microtubule subpopulations in qualitatively different manners. Implications for neurodegeneration. *J Biol Chem* 280: 13520-8
- Li W, Miki T, Watanabe T, Kakeno M, Sugiyama I, Kaibuchi K, Goshima G (2011) EB1 promotes microtubule dynamics by recruiting Sentin in *Drosophila* cells. *J Cell Biol* 193: 973-83
- Li W, Moriwaki T, Tani T, Watanabe T, Kaibuchi K, Goshima G (2012) Reconstitution of dynamic microtubules with *Drosophila* XMAP215, EB1, and Sentin. *J Cell Biol* 199: 849-62
- Liu Y, Wang C, Destin G, Szaro BG (2015) Microtubule-associated protein tau promotes neuronal class II beta-tubulin microtubule formation and axon elongation in embryonic *Xenopus laevis*. *Eur J Neurosci* 41: 1263-75
- Lowery LA, Faris AER, Stout A, Van Vactor D (2012) Neural explant cultures from *Xenopus laevis*. *JoVE*: e4232
- Lowery LA, Stout A, Faris AE, Ding L, Baird MA, Davidson MW, Danuser G, Van Vactor D (2013) Growth cone-specific functions of XMAP215 in restricting microtubule dynamics and promoting axonal outgrowth. *Neural Dev* 8: 22
- Luo L, Liao YJ, Jan LY, Jan YN (1994) Distinct morphogenetic functions of similar small GTPases: *Drosophila* Drac1 is involved in axonal outgrowth and myoblast fusion. *Genes Dev* 8: 1787-1802
- Manna T, Grenningloh G, Miller HP, Wilson L (2007) Stathmin family protein SCG10 differentially regulates the plus and minus end dynamics of microtubules at steady state *in vitro*: implications for its role in neurite outgrowth. *Biochemistry* 46: 3543-52
- Manna T, Thrower DA, Honnappa S, Steinmetz MO, Wilson L (2009) Regulation of microtubule dynamic instability *in vitro* by differentially phosphorylated stathmin. *J Biol Chem* 284: 15640-9
- Marner L, Nyengaard JR, Tang Y, Pakkenberg B (2003) Marked loss of myelinated nerve fibers in the human brain with age. *J Comp Neurol* 462: 144-52
- Maurer SP, Cade NI, Bohner G, Gustafsson N, Boutant E, Surrey T (2014) EB1 accelerates two conformational transitions important for microtubule maturation and dynamics. *Curr Biol* 24: 372-84
- Monroy BY, Tan TC, Oclaman JM, Han JS, Simó S, Niwa S, Nowakowski DW, McKenney RJ, Ori-Mckenney KM (2020) A combinatorial MAP code dictates polarized microtubule transport. *Dev Cell* 53
- Mortuza GB, Cavazza T, Garcia-Mayoral MF, Hermida D, Peset I, Pedrero JG, Merino N, Blanco FJ, Lyngsø J, Bruix M, Pedersen JS, Vernos I, Montoya G (2014) XTACC3–XMAP215 association reveals an asymmetric interaction promoting microtubule elongation. *Nature Communications* 5: 5072
- Nieuwkoop, J. F (1994) *Normal table of Xenopus laevis (Daudin): A systematical and chronological survey of the development from the fertilized egg till the end of metamorphosis*. Garland Pub. Inc. , New York
- Nwagbara BU, Faris AE, Bearce EA, Erdogan B, Ebbert PT, Evans MF, Rutherford EL, Enzenbacher TB, Lowery LA (2014) TACC3 is a microtubule plus-end tracking protein that

- hr/>
- promotes axon elongation and also regulates microtubule plus-end dynamics in multiple embryonic cell types. *Mol Biol Cell*
- O'Neill EM, Rebay I, Tjian R, Rubin GM (1994) The activities of two Ets-related transcription factors required for Drosophila eye development are modulated by the Ras/MAPK pathway. *Cell* 78: 137-47.
- Panda D, Goode BL, Feinstein SC, Wilson L (1995) Kinetic stabilization of microtubule dynamics at steady state by tau and microtubule-binding domains of tau. *Biochemistry* 34: 11117-27
- Prokop A (2013) A rough guide to Drosophila mating schemes. *figshare*: [dx.doi.org/10.6084/m9.figshare.106631](https://doi.org/10.6084/m9.figshare.106631)
- Prokop A (2020) Cytoskeletal organization of axons in vertebrates and invertebrates. *J Cell Biol* 219: e201912081
- Prokop A, Beaven R, Qu Y, Sánchez-Soriano N (2013) Using fly genetics to dissect the cytoskeletal machinery of neurons during axonal growth and maintenance. *J Cell Sci* 126: 2331-41
- Prokop A, Küppers-Munther B, Sánchez-Soriano N (2012) Using primary neuron cultures of Drosophila to analyse neuronal circuit formation and function. *The making and un-making of neuronal circuits in Drosophila* 69: 225-47
- Prokop A, Meinertzhagen IA (2006) Development and structure of synaptic contacts in Drosophila. *Semin Cell Dev Biol* 17: 20-30
- Qiang L, Sun X, Austin TO, Muralidharan H, Jean DC, Liu M, Yu W, Baas PW (2018) Tau does not stabilize axonal microtubules but rather enables them to have long labile domains. *Curr Biol* 28: 2181-2189 e4
- Qiang L, Yu W, Andreadis A, Luo M, Baas PW (2006) Tau protects microtubules in the axon from severing by katanin. *J Neurosci* 26: 3120-9
- Qu Y (2015) Novel concepts of microtubule regulation during axon growth and maintenance. *Faculty of Life Sciences PhD*: 205
- Qu Y, Hahn I, Lees M, Parkin J, Voelzmann A, Dorey K, Rathbone A, Friel C, Allan V, Okenve Ramos P, Sánchez-Soriano N, Prokop A (2019) Efa6 protects axons and regulates their growth and branching by inhibiting microtubule polymerisation at the cortex. *eLife* 8: e50319
- Qu Y, Hahn I, Webb SED, Pearce SP, Prokop A (2017) Periodic actin structures in neuronal axons are required to maintain microtubules. *Mol Biol Cell* 28 296-308
- Ramirez-Rios S, Denarier E, Prezel E, Vinit A, Stoppin-Mellet V, Devred F, Barbier P, Peyrot V, Sayas CL, Avila J, Peris L, Andrieux A, Serre L, Fourest-Lievain A, Arnal I (2016) Tau antagonizes end-binding protein tracking at microtubule ends through a phosphorylation-dependent mechanism. *Mol Biol Cell* 27: 2924-2934
- Rogers SL, Rogers GC, Sharp DJ, Vale RD (2002) Drosophila EB1 is important for proper assembly, dynamics, and positioning of the mitotic spindle. *J Cell Biol* 158: 873-84
- Roostalu J, Cade NI, Surrey T (2015) Complementary activities of TPX2 and chTOG constitute an efficient importin-regulated microtubule nucleation module [corrigendum: same issue, p.1512]. *Nat Cell Biol* 17: 1422-34
- Roostalu J, Thomas C, Cade NI, Kunzelmann S, Taylor IA, Surrey T (2020) The speed of GTP hydrolysis determines GTP cap size and controls microtubule stability. *eLife* 9
- Sánchez-Soriano N, Gonçalves-Pimentel C, Beaven R, Haessler U, Ofner L, Ballestrém C, Prokop A (2010) Drosophila growth cones: a genetically tractable platform for the analysis of axonal growth dynamics. *Dev Neurobiol* 70: 58-71
- Sánchez-Soriano N, Travis M, Dajas-Bailador F, Gonçalves-Pimentel C, Whitmarsh AJ, Prokop A (2009) Mouse ACF7 and Drosophila Short stop modulate filopodia formation and microtubule organisation during neuronal growth. *J Cell Sci* 122: 2534-42

- Sayas CL, Tortosa E, Bollati F, Ramirez-Rios S, Arnal I, Avila J (2015) Tau regulates the localization and function of End-binding proteins 1 and 3 in developing neuronal cells. *J Neurochem* 133: 653-67
- Schaedel L, John K, Gaillard J, Nachury MV, Blanchoin L, Thery M (2015) Microtubules self-repair in response to mechanical stress. *Nat Mater* 14: 1156-63
- Sive HL, Grainger RM, Harland RM (2010) Microinjection of Xenopus oocytes. *Cold Spring Harb Protoc* 2010: pdb prot5536
- Slater PG, Cammarata GM, Samuelson AG, Magee A, Hu Y, Lowery LA (2019) XMAP215 promotes microtubule-F-actin interactions to regulate growth cone microtubules during axon guidance. *J Cell Sci*: jcs.224311
- Strumpf D, Volk T (1998) Kakapo, a novel *Drosophila* protein, is essential for the restricted localization of the neuregulin-like factor, Vein, at the muscle-tendon junctional site. *J Cell Biol* 143: 1259-1270
- Takei Y, Teng J, Harada A, Hirokawa N (2000) Defects in axonal elongation and neuronal migration in mice with disrupted tau and map1b genes. *J Cell Biol* 150: 989-1000
- Tang Q, Rui M, Bu S, Wang Y, Chew LY, Yu F (2020) A microtubule polymerase is required for microtubule orientation and dendrite pruning in *Drosophila*. *EMBO J* 39: e103549
- Thawani A, Kadzik RS, Petry S (2018) XMAP215 is a microtubule nucleation factor that functions synergistically with the  $\gamma$ -tubulin ring complex. *Nature Cell Biology* 20: 575-585
- Tymanskyj SR, Scales TM, Gordon-Weeks PR (2012) MAP1B enhances microtubule assembly rates and axon extension rates in developing neurons. *Mol Cell Neurosci* 49: 110-19
- van der Vaart B, Franker MA, Kuijpers M, Hua S, Bouchet BP, Jiang K, Grigoriev I, Hoogenraad CC, Akhmanova A (2012) Microtubule Plus-End Tracking Proteins SLAIN1/2 and ch-TOG Promote Axonal Development. *J Neurosci* 32: 14722-8
- Vemu A, Szczesna E, Zehr EA, Spector JO, Grigorieff N, Deaconescu AM, Roll-Mecak A (2018) Severing enzymes amplify microtubule arrays through lattice GTP-tubulin incorporation. *Science* 361: eaau1504
- Villarreal-Campos D, Gonzalez-Billault C (2014) The MAP1B case: an old MAP that is new again. *Dev Neurobiol* 74: 953-71
- Voelzmann A, Hahn I, Pearce S, Sánchez-Soriano NP, Prokop A (2016) A conceptual view at microtubule plus end dynamics in neuronal axons. *Brain Res Bulletin* 126: 226-37
- Voelzmann A, Liew Y-T, Qu Y, Hahn I, Melero C, Sánchez-Soriano N, Prokop A (2017) *Drosophila* Short stop as a paradigm for the role and regulation of spectraplakins. *Sem Cell Dev Biol* 69: 40-57
- Wieczorek M, Bechstedt S, Chaaban S, Brouhard GJ (2015) Microtubule-associated proteins control the kinetics of microtubule nucleation. *Nat Cell Biol* 17: 907-16
- Wu X, Kodama A, Fuchs E (2008) ACF7 regulates cytoskeletal-focal adhesion dynamics and migration and has ATPase activity. *Cell* 135: 137-48
- Yang N, Inaki M, Cliffe A, Rørth P (2012) Microtubules and Lis-1/NudE/dynein regulate invasive cell-on-cell migration in *Drosophila*. *PLoS One* 7: e40632
- Zanic M, Stear JH, Hyman AA, Howard J (2009) EB1 recognizes the nucleotide state of tubulin in the microtubule lattice. *PloS one* 4: e7585-e7585
- Zanic M, Widlund PO, Hyman AA, Howard J (2013) Synergy between XMAP215 and EB1 increases microtubule growth rates to physiological levels. *Nat Cell Biol* 15: 688-693



## Figures

**Fig. 1.** Eb1, Msps and Tau share the same combination of axonal loss-of-function phenotypes *Drosophila* in primary neurons. **A-H)** Images of representative examples of pre-cultured embryonic primary neurons either immuno-stained for Eb1 (top) or for tubulin (bottom); neurons were either wild-type controls (ctrl) or carried the mutant alleles *msps*<sup>1</sup>, *tau*<sup>KO</sup> or *Eb1*<sup>04524</sup> in homozygosis (from left to right); asterisks indicate cell bodies, black arrow heads the axon tips, white arrow heads point at areas of MT disorganisation, dashed squares in A-D are shown as 3.5-fold magnified close-ups below each image with black arrows pointing at Eb1 comets; the axonal outline in D is indicated by a dotted line; scale bar in A represents 15 µm in all images. **I-N)** Quantification of different parameters (as indicated above each graph) obtained from pre-cultured embryonic primary neurons with the same genotypes as shown in A-H. Sample numbers, and P-values obtained with Kruskal-Wallis ANOVA test for the different genotypes are indicated in each graph. Error bars represent median ± 95% confidence interval (I - M) or mean ± SEM (N). For raw data see Tab. T1.

**Fig. 1-S1.** A candidate screen of axonal loss-of-function phenotypes in primary neurons. Graphs show extended data sets for four of the parameters displayed in Fig. 1 (indicated above each graph). Data points/bars representing mutant conditions for different genes are consistently colour-coded in all graphs, and conditions used are indicated below (6HIV, cultured from embryos for 6hrs; 6dpre, cultured from embryos for 12hrs following 6 day pre-culture; L3, cultured from late larval CNS for 18hrs). Allele names are given as superscript: no slash indicates homozygous, a present slash hetero-allelic conditions. Data were normalised to parallel controls (dashed horizontal line) and are shown as median ± 95% confidence interval (B,C) or mean ± SEM (A,D); merged sample numbers from at least two experimental repeats consisting of 3 samples each are shown at the bottom, P-values obtained with Kruskal-Wallis ANOVA test above data points/bars. For raw data see Tab. T1-S1.

**Fig. 1-S2.** Correlation of different Eb1 comet properties. **A,B)** Eb1 amount at comets is calculated as the product of comet length (A) and the fluorescent mean intensity of Eb1 comets (B), which are both to similar degrees affected by homozygous condition of *msps*<sup>A</sup>, *tau*<sup>KO</sup> and *Eb1*<sup>04524</sup> in embryo derived neurons cultured for 12hrs following 6 day pre-culture (6dpre); data were normalised to controls (dashed horizontal line) and are shown as median ± 95% confidence interval; merged sample numbers from at least three experimental repeats are shown at the bottom, P-values obtained with Kruskal-Wallis ANOVA test above data points. **C)** Table lists data for Eb1 amounts (fixed neurons; compare Fig.1E-H, L) or for comet velocity/lifetime (live imaging; compare Fig.1M,N), all obtained from pre-cultured embryonic primary neurons carrying the same combinations of mutant alleles (indicated on the left; used alleles: *tub84B*<sup>def</sup>, *msps*<sup>A</sup>, *tau*<sup>KO/Df</sup>, *eb1*<sup>04524</sup>, *star*<sup>KO</sup>). **D,E)** Plotting comet velocity or lifetime against Eb1 amounts from different genetic conditions shows a fairly good correlation (r and p-value determined via non-parametric Spearman correlation analysis). For raw data see Tab. T1-S2.

**Fig. 2.** *Eb1*, *tau* and *msps* interact genetically. **A-B")** Axon length, MT disorganisation and Eb1



amount (as indicated on the right), for primary neurons displaying heterozygous (A-A', larval cultures) and homozygous (B-B', embryonic 6d pre-cultures') mutant conditions, alone or in combination. Data were normalised to parallel controls (dashed horizontal lines) and are shown as median  $\pm$  95% confidence interval (A, A', B, B') or mean  $\pm$  SEM (A', B'); merged sample numbers from at least two independent repeats of 3 parallel setups are shown at the bottom, P-values obtained with Kruskal-Wallis ANOVA test above data points/bars; used alleles: *msps*<sup>A</sup>, *tau*<sup>KO</sup>, *Eb1*<sup>04524</sup>. **C**) Green dots represent data for MT disorganisation (from A', B') plotted against Eb1 amounts (from B', B'' as well as Fig.1J,L, Fig.1-S1B,D), purple dots show comparable data obtained from larval primary neurons (from Fig.A', A', Fig.1-S1B,D), and black dots similar data obtained from primary *Xenopus* neurons (Fig.G,H); r and p-value determined via non-parametric Spearman correlation analysis; see further detail of these correlations in Fig.2-S2. For raw data see Tab. T2.

**Fig. 2-S1.** Genetic interactions and heterozygous combinations. Graphs show data sets extending on data displayed in Fig. 2 for heterozygous mutant conditions. **A**) Eb1 comet numbers in fixed primary neurons cultured for 12hrs following 5 day pre-culture. **B**) Comet velocity and lifetime obtained from live analyses of primary neurons cultured for 18hrs from late larval CNSs. In all graphs, data were normalised to parallel controls (dashed horizontal lines) and are shown as median  $\pm$  95% confidence interval (B) or mean  $\pm$  SEM (A); merged sample numbers from at least two experimental repeats are shown at the bottom, P-values obtained with Kruskal-Wallis ANOVA test above data points/bars; used alleles: *msps*<sup>A</sup>, *tau*<sup>KO</sup>, *Eb1*<sup>04524</sup>. For raw data see Tab. T2-S1.

**Fig. 2-S2.** Increasing Eb1 amounts correlate with decreasing MT disorganisation. The data and graph show further details behind the correlations displayed in Fig.2C. **A**) The table shows for different allelic combinations and culture conditions (indicated in 2<sup>nd</sup> column; 6HIV, cultured from embryos for 6hrs; 6d pre, cultured from embryos for 12hrs following 6 day pre-culture; L3, cultured from late larval CNS for 18hrs) the respective Eb1 amounts (3<sup>rd</sup> column) and MT disorganisation (4<sup>th</sup> column), as obtained from different sets of experiments throughout this work (5<sup>th</sup> column lists the figures from where these data originate); numbers in the 1<sup>st</sup> column correspond to numbers of data points in the graph in B. **B**) Correlation plot of the data shown in A, with numbers and colours of data points corresponding to the 1<sup>st</sup> column; r and p-value determined via non-parametric Spearman correlation analysis. For raw data see Tab. T2-S2.

**Fig. 3.** Eb1, Msps and Tau functionally interact in the fly brain and in frog primary neurons. **A,B**) Medulla region of adult brains at 26-27 days after eclosure, all carrying the *GMR31F10-Gal4* driver and *UAS-GFP- $\alpha$ -tubulin84B* (*GMR-tub*) which together stain MTs in a subset of lamina neuron axons that terminate in the medulla; the further genetic background is either wild-type (A) or triple-heterozygous (*Eb1*<sup>04524/+</sup> *msps*<sup>A/+</sup> *tau*<sup>KO/KO</sup>; B); white/black arrows indicate axonal swellings without/with MT disorganisation; rectangles outlined by red dashed lines are shown as 2.5 fold magnified insets where white arrow heads point at disorganised MTs. **C,D**) Quantitative analyses of specimens shown in A and B with respect to the number of axonal swelling (C) and swellings with MT disorganisation (D); bars show mean  $\pm$  SEM; P values from Kruskal-Wallis one-way tests are given above each column, merged sample numbers (i.e. individual axon bundles) from at least two experimental repeats at the bottom of each bar. **E**-

**F'''') Primary *Xenopus* neurons stained either for tubulin (tub; top; white arrows indicating unbundled MTs, white arrowheads unbundled areas with MT disorganisation), black arrows comets labelled with MACF43::GFP (MACF43; visible as black spots); blacks dashed squares in E-E''' and F-F''' shown as 2.5 fold magnified close-ups below; ↓ behind gene symbols indicates 50% knock-down thus approximating heterozygous conditions. **G,H)** Quantification of specimens shown in E-F''' with respect to MT disorganisation (G) and comet MACF43::GFP amount (H); data were normalised to parallel controls (dashed horizontal lines) and are shown as mean ± SEM (G) or median ± 95% confidence interval (H); merged sample numbers from at least two experimental repeats are shown at the bottom, P-values obtained with Kruskal-Wallis ANOVA test above data points/bars. The scale bar in A represents 15 µm in A,B and 20 µm in E-F'''. For raw data see Tab. T3.**

**Fig. 3-S1.** Support data for *Xenopus* experiments. **A-B')** A RT-PCR DNA gel/Western blot and their quantifications showing the degrees of EB3/Tau knock-downs upon application of different morpholino concentrations (indicated on top in blots and at the bottom in graphs), using ODC1 and β-actin as loading controls; data are normalised to no-morpholino controls from two experimental repeats (dashed lines). 50% knock-down of XMAP215 was achieved by injecting 6 ng of the validated XMAP215 MO as described previously (Lowery et al., 2013, Slater et al., 2019). **C-G)** Different properties of MACF43::GFP comets (as indicated upon graphs) obtained from *Xenopus* primary neurons, either upon 50% (C,D) or 70% (E-G) knock-down of respective genes (indicated as 50/70%KD); data were normalised to parallel controls (dashed horizontal lines) and are shown as median ± 95% confidence interval; merged sample numbers from at least two experimental repeats are shown at the bottom, P-values obtained with Kruskal-Wallis ANOVA and Dunn's posthoc test above data points. For raw data see Tab. T3-S1.

**Fig. 4.** Eb1 and Msps depend on each other for MT plus end localisation. **A-A'')** Primary neurons at 6HIV co-expressing Eb1::mCherry (magenta, Eb1) and Msps<sup>FL</sup>::GFP (green, Msps) and imaged live; asterisks indicate somata, scale bar represents 10µm, dashed boxes indicate the positions of the 3.5-fold magnified close-ups shown at the bottom with arrowheads pointing at the position of Msps::GFP accumulation (same in C,C'). **B,B')** Kymograph of live movies (as in A-A'') with the dashed line on the left representing the dashed lines shown in A' and A'' (i.e. the length of the axon; proximal at the top) and the x-axis indicating time; arrowheads point at trajectories of Msps and Eb1 which are almost identical. **C)** Primary neurons expressing Msps::GFP and imaged live, either displaying wild-type background (ctrl) or being homozygous mutant for *Eb1*<sup>04524</sup> (*Eb1*<sup>-/-</sup>); white arrowheads point at Msps::GFP comets which are much smaller in the mutant neurons. **D)** Schematic representations of Msps<sup>FL</sup>::GFP and Msps<sup>ΔCTD</sup>::GFP. **D',D'')** Graphs displaying axon length and MT disorganisation (as indicated) for pre-cultured embryonic primary neurons expressing GFP or Msps::GFP constructs via the *elav-Gal4* driver, either in wild-type or *msps*<sup>Δ/1</sup> mutant background; data were normalised to parallel controls (dashed horizontal lines) and are shown as median ± 95% confidence interval (D') or mean ± SEM (D''); merged sample numbers from at least two experimental repeats are shown at the bottom, P-values obtained with Kruskal-Wallis ANOVA test above data points/bars. **E)** Model view of the results shown here and in Fig. 1; for explanations see main text and Discussion. For raw data see Tab. T4.

**Fig. 4-S1.** Loss of Tacc or Sentin does not cause obvious axonal phenotypes. Axon length (**A**) and MT disorganisation (**B**) for primary neurons at 6HIV which were either wild-type (wt) or homozygous mutant for *sentin* or *dTACC* (as indicated); data were normalised to parallel controls (dashed horizontal lines) and are shown as median  $\pm$  95% confidence interval (A) or mean  $\pm$  SEM (B); merged sample numbers from at least two experimental repeats are shown at the bottom, P-values obtained with Kruskal-Wallis ANOVA test above data points/bars. For raw data see Tab. T4-S1.

**Fig. 5.** Tau promotes Eb1 pools at MT plus ends by outcompeting its association with the MT lattice. **A-A'')** Example of neuron imaged live with disorganised MTs to illustrate Tau binding (green) along the MT lattice, separated from Eb1 comets (magenta); asterisks indicate somata, the scale bar represents 10 $\mu$ m, dashed boxes indicate the positions of the 4fold magnified close-ups shown at the bottom, white arrowheads point at Eb1 comets (same in B-D). **B-D)** Primary neurons at 6HIV stained for Eb1 which are either wild-type (B), *tau*<sup>KO/Df</sup> mutant (C) or *tau*<sup>KO/Df</sup> mutant plus expressing Eb1::GFP driven by *elav-Gal4* (D); white/red arrowheads indicate Eb1 comets/lattice localisation. **E-I)** Different parameters (as indicated) of control (ctrl) or *tau*<sup>KO/Df</sup> (*tau*<sup>-/-</sup>) mutant neurons without/with *elav-Gal4*-driven expression of Eb1::GFP or Shot-Ctail::GFP (as indicated); data were normalised to parallel controls (dashed horizontal lines) and are shown as mean  $\pm$  SEM (I) or median  $\pm$  95% confidence interval (E-H); merged sample numbers from at least two independent repeats with 3 experimental setups each are shown at the bottom, P-values obtained with Kruskal-Wallis ANOVA and Dunn's posthoc test above data points/bars. **J)** Model view of the results shown here; for explanations see main text and Discussion. For raw data see Tab. T5.

**Fig. 5-S1** Upon tau deficiency, GTP-tubulin is reduced at MT plus ends but unchanged at lattices. **A-B'')** Fixed primary neurons stained for Eb1 (magenta) and GTP-tubulin (green); asterisks indicate somata, scale bar represents 10 $\mu$ m, dashed boxes indicate the positions of the 4fold magnified close-ups shown at the bottom, arrowheads point at Eb1::GFP comets and GTP caps. **C,D)** Graphs showing staining intensity of GTP-tubulin at MT plus ends (C) and along the MT lattice (D), and that *msps*<sup>A/146</sup> mutant phenotypes were not rescued by Eb1::GFP expression (C,D). **E)** Graphs showing staining intensity of Eb1 along the MT lattice of neurons without/with *elav-Gal4*-driven expression of *dtau*. Overexpression of *dtau* leads to a reduction of Eb1 at the MT shaft; data were normalised to parallel controls (dashed horizontal lines) and are shown as median  $\pm$  95% confidence interval; merged sample numbers from at least two independent repeats with 3 experimental setups each are shown at the bottom, P-values obtained with Kruskal-Wallis ANOVA test above data points/bars. For raw data see Tab. T5-S1.

**Fig. 5-S2** Eb1 overexpression does not rescue *msps* mutant phenotypes. Graphs show that Eb1 lattice localisation is unaffected by loss of Msps in primary neurons at 6HIV (A) or at ~12HIV following 6 day preculture (B). Staining intensity of GTP-tubulin at MT plus ends is reduced in *msps*<sup>A/A</sup> and *Eb1*<sup>04524/04524</sup> mutant at 6dpre (C). Expressing Eb1::GFP via *elav-Gal4* does not rescue comet velocities (D), comet lifetime  $\epsilon$  and MT disorganisation (F) in primary neurons of *msps*<sup>A/146</sup> mutants (cultured 12HIV following 6 day preculture); data were normalised to parallel controls (dashed horizontal lines) and are shown as mean  $\pm$  SEM (F) or median  $\pm$  95% confidence interval (A-E); merged sample numbers from at least two experimental repeats are shown at the bottom, P-values obtained with Kruskal-Wallis ANOVA test with Dunn's posthoc analysis above data points/bars. For raw data see Tab. T5-S2

**Fig. 6.** Shot-mediated guidance as a mechanism linking Eb1 at MT plus ends to bundle organisation. **A)** Schematic representation of Shot constructs (CH, actin-binding calponin-homology domains; EF, EF-hand motifs; GRD, MT-binding Gas2-related domain; Ctail, unstructured MT-binding domain containing Eb1-binding SxIP motifs in blue); in Shot-3MTLS\*::GFP the SxIP motifs are mutated. **B)** Fixed primary larval neurons at 18HIV obtained from late larval CNS stained for GFP (green) and tubulin (magenta), which are either wild-type (top) or *Eb1*<sup>04524/+</sup>*mmps*<sup>A/+</sup>*tau*<sup>KO/+</sup> triple-heterozygous (indicated on right) expressing GFP or either of the constructs shown in D; scale bar 10µm. **C)** Quantification of MT disorganisation of neurons as shown in B. **D,E)** MT disorganisation in *shot*<sup>3/3</sup>*Eb1*<sup>04524/04524</sup> double-mutant neurons is not enhanced over single mutant conditions assessed in fixed primary neurons at 6HIV (D) or 12HIV following 6 day pre-culture (E). In all graphs data were normalised to parallel controls (dashed horizontal lines) and are shown as mean ± SEM; merged sample numbers from at least two independent repeats with 3 experimental setups each are shown at the bottom, P-values obtained with Kruskal-Wallis ANOVA test above bars. **F,F')** Model derived from previous work (Alves-Silva et al., 2012), proposing that the spectraplakine Shot cross-links Eb1 at MT plus ends with cortical F-actin, thus guiding MT extension in parallel to the axonal surface.

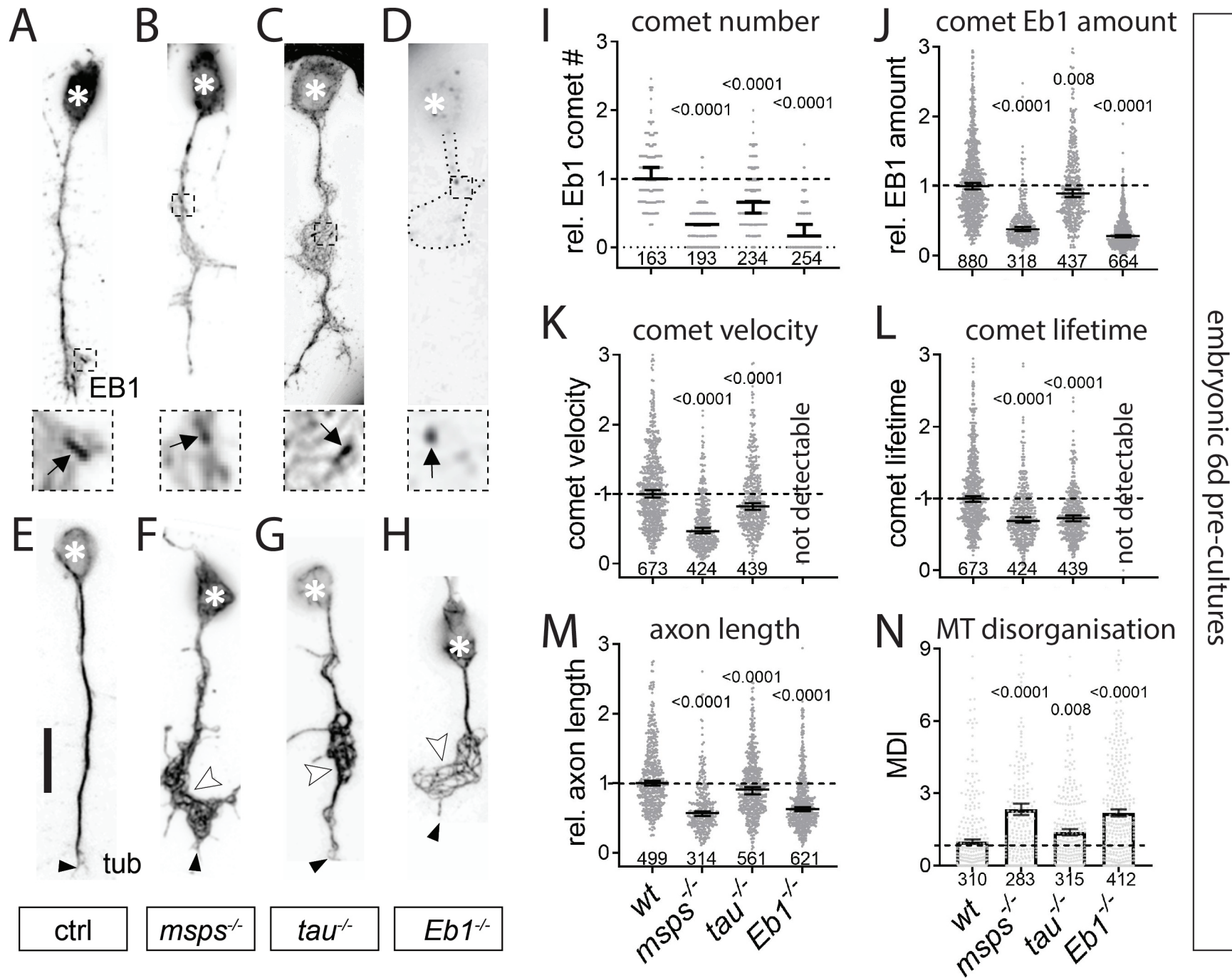
**Fig. 7.** Model summarising the common functional pathway of Eb1, Msps and Tau. Images on the left show functional diagrams and on the right cartoon models for wild-type and four mutant conditions as indicated. **A,A')** In wild-type (WT) neurons, the three factors bind independently to MTs: Msps to the very tip of plus ends, Eb1 to the GTP-cap (GTP-tubulin shown with yellow dots) but lagging behind the front, and Tau along the lattice. Tau promotes Eb1 pools at MT plus ends (green arrow in A) by outcompeting its binding along the lattice (green T-bar in A'). Eb1 and Msps mutually promote each other's localisation (stippled black and red arrows in A, A'): Msps is the main promoter of polymerisation (brown arrow), thus sustaining a prominent GTP-tubulin cap (pale yellow box in A) for Eb1; Eb1 potentially promotes sheet formation of protofilaments at the plus tip (red arrow), thus helping Msps to bind; Eb1 links to Shot (orange double-arrow) which provides MT plus end guidance (blue dashed arrow). **B,B')** Upon loss of Eb1, the plus end sheet structure is weakened, thus weakening Msps binding and, in turn, reducing polymerisation (thinner/shorter arrows, smaller font); Shot detaches, thus abolishing guidance (curved off-track extension arrow). **C,C')** Upon loss of Msps, its catalysis of polymerisation is abolished, the GTP-tubulin cap shrinks, less Eb1 binds, thus strongly weakening Shot binding and guidance. **D,D')** Upon loss of Tau, Eb1 is recruited to the MT lattice, thus reducing its plus end amounts; reduced Eb1 negatively impacts on Shot and Msps causing the milder guidance and polymerisation effects we observed. **E,E')** Upon loss of Shot, the localisation of the other three proteins is unaffected, but guidance is abolished.

**Movie M1.** Msps::GFP and Eb1::RFP jointly track MT plus ends. Live movie of a wild-type neuron co-expressing Msps::GFP and Eb1::RFP; for stills see Fig.4A-B'. As indicated, single channels are shown on the left and middle, and the combined movie on the right. The movie was acquired at 0.5 frames per second, and play at 0.5 s per frame. The scale bar indicates 10 µm.

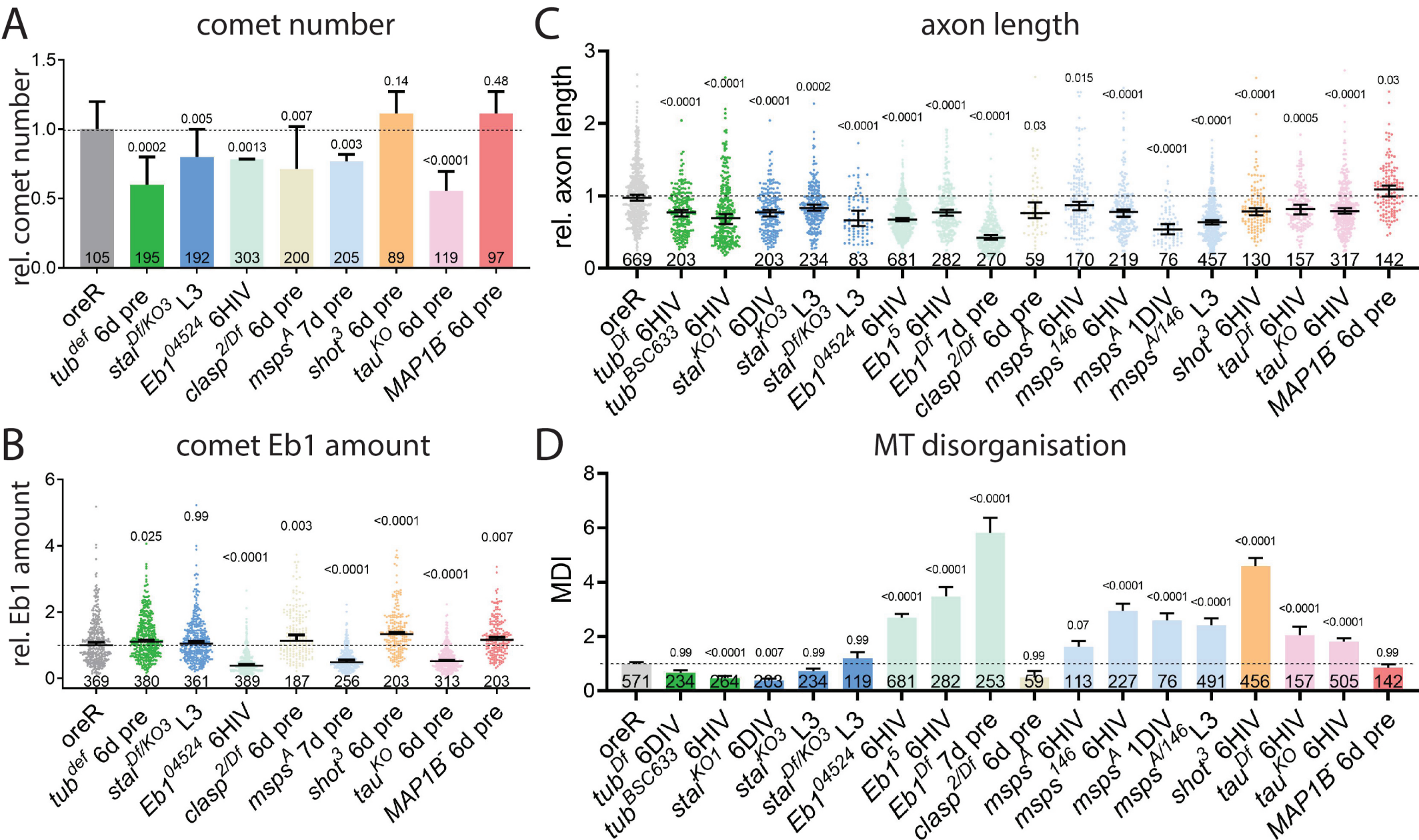
**Movie M2.** Msps plus end localisation in wild-type neurons. Live movie of a wild-type neuron expressing Msps::GFP; for stills see Fig.4C. The movie was acquired at 1 frame per second, and plays at 0.2 s per frame. The scale bar indicates 10 µm.

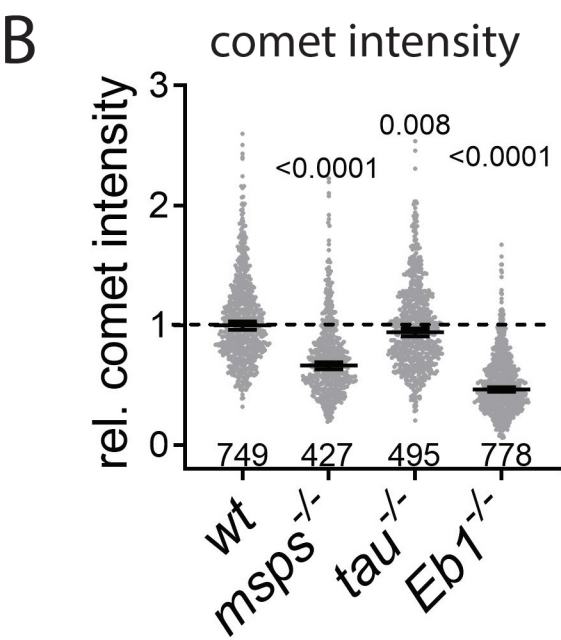
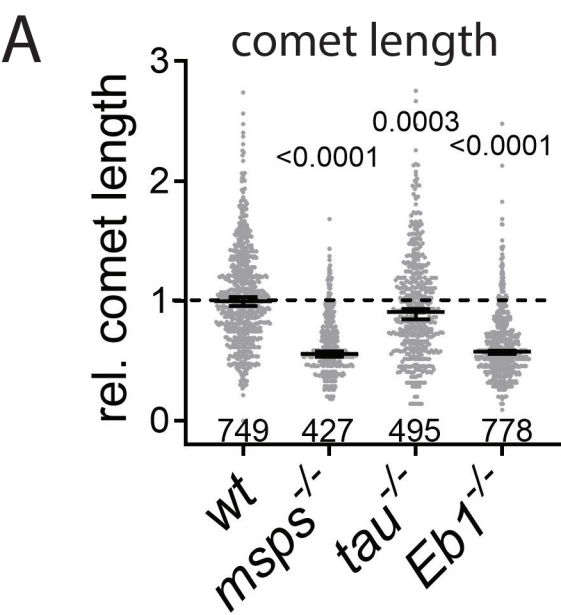


1183 **Movie M3.** Msps plus end localisation is impaired in the absence of Eb1. Live movie of an  
1184 *Eb1*<sup>04524/04524</sup> mutant neuron expressing Msps::GFP; for stills see Fig.4C'. The movie was  
1185 acquired at 1 frames per second, and plays at 0.2 s per frame. The scale bar indicates 10 µm.



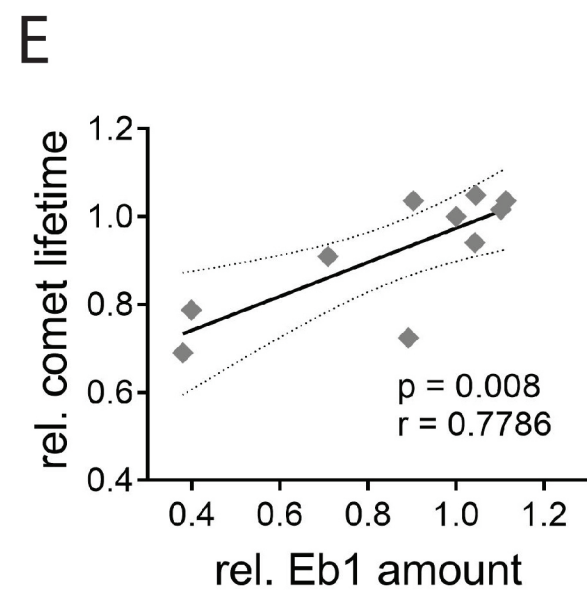
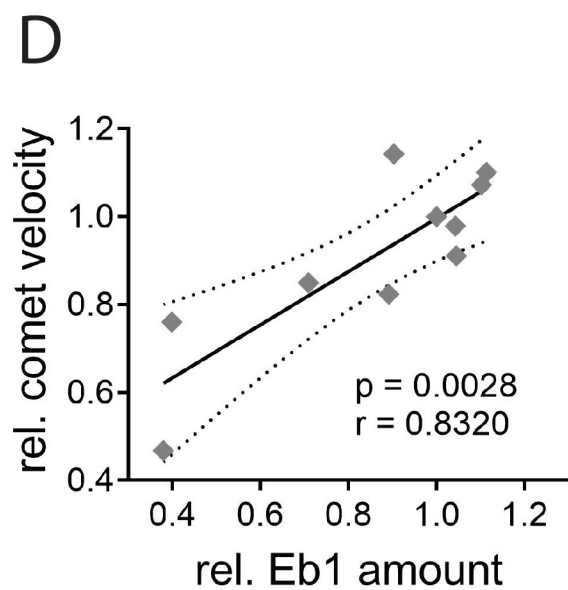
Hahn et al. Fig. 1



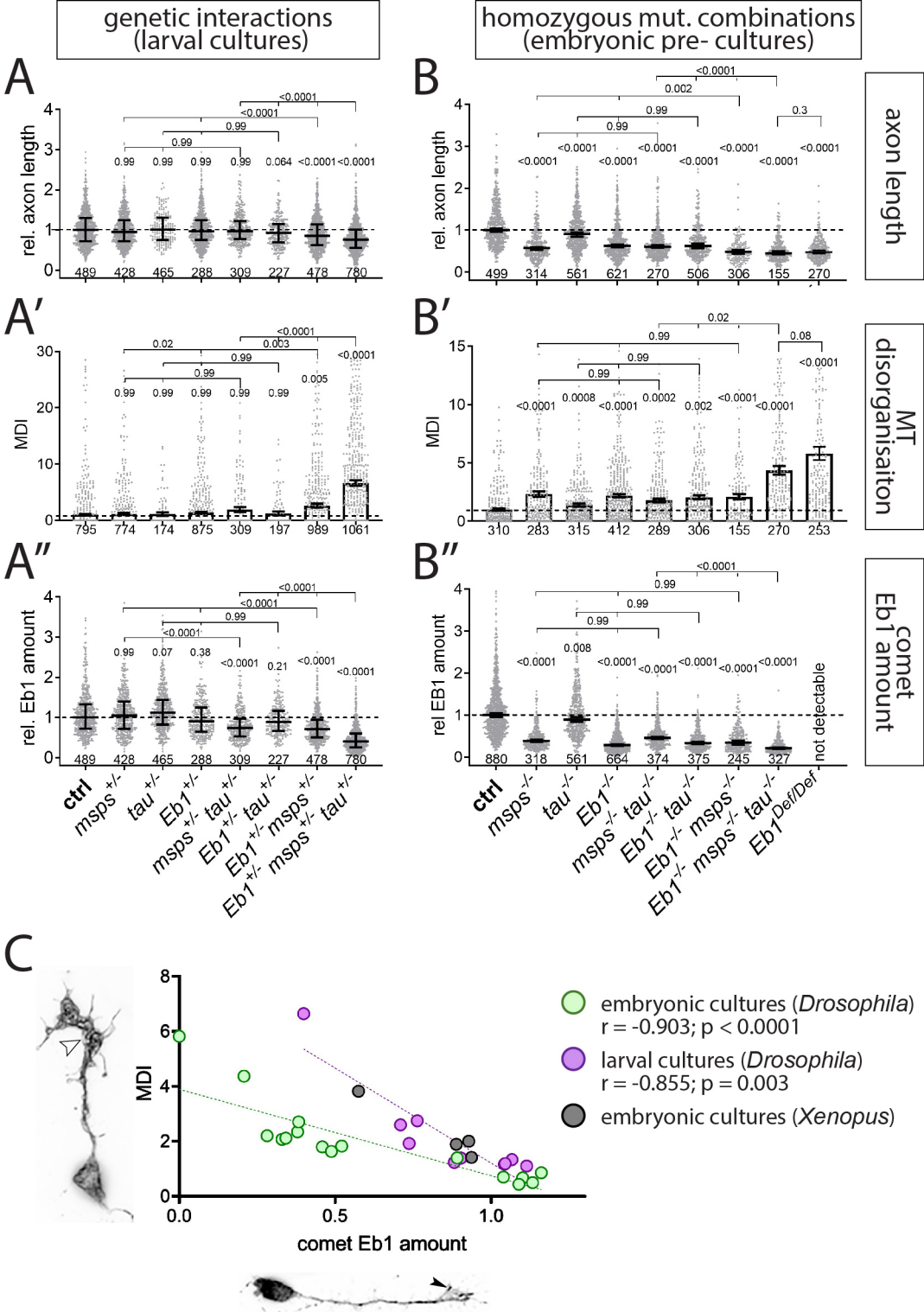


**C**

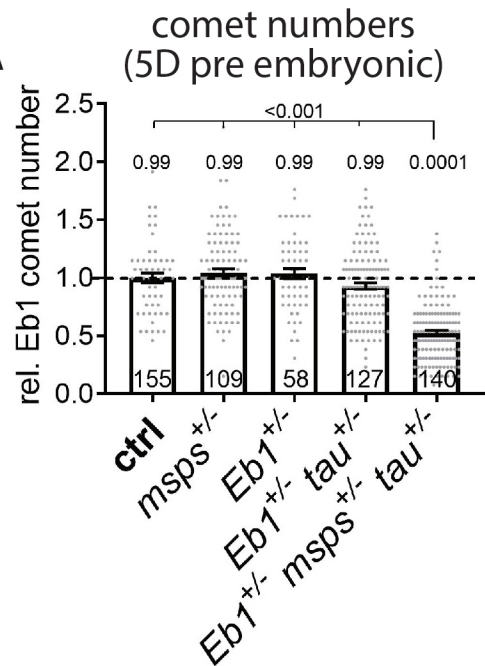
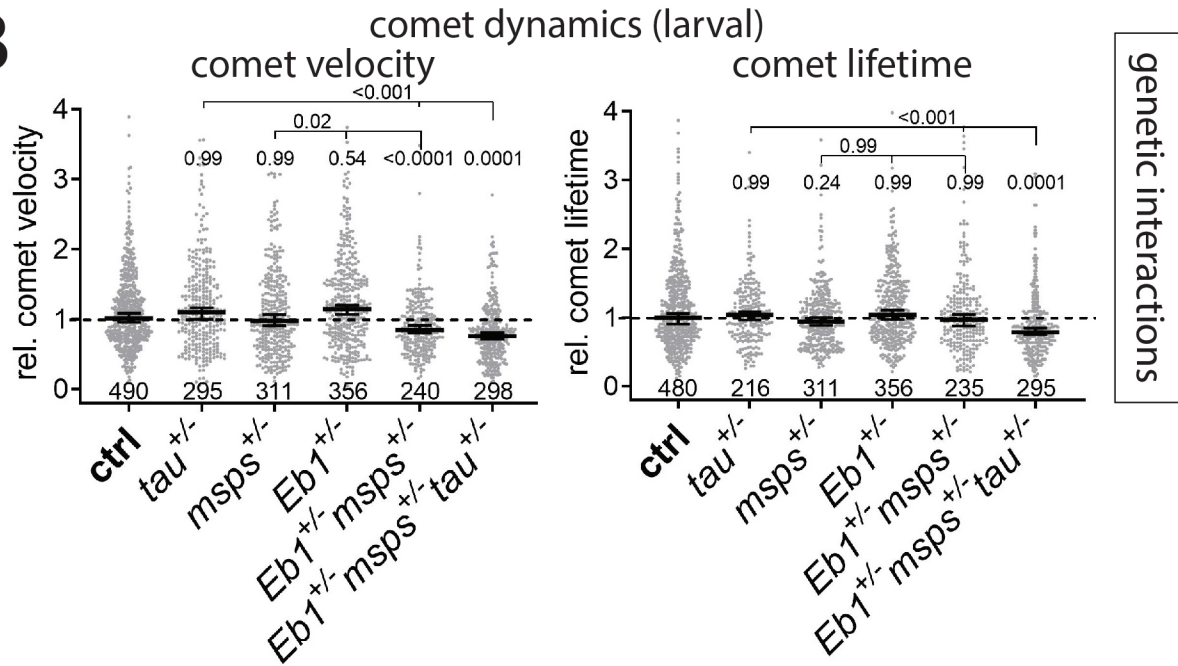
	Eb1 amount	comet velocity	comet lifetime
ctrl	1.0000	1.0000	1.0000
tau+/-	1.1130	1.1010	1.0360
msps+/-	1.0430	0.9792	0.9411
eb1+/-	0.9028	1.1430	1.0360
eb1+/- msp+/-	0.7093	0.8496	0.9097
eb1+/- msp+/- tau+/-	0.3989	0.7602	0.7879
msps-/-	0.3796	0.4676	0.6905
tau-/-	0.8918	0.8234	0.7246
tubdef/def	1.1020	1.0720	1.0160
stai-/-	1.0450	0.9107	1.0490







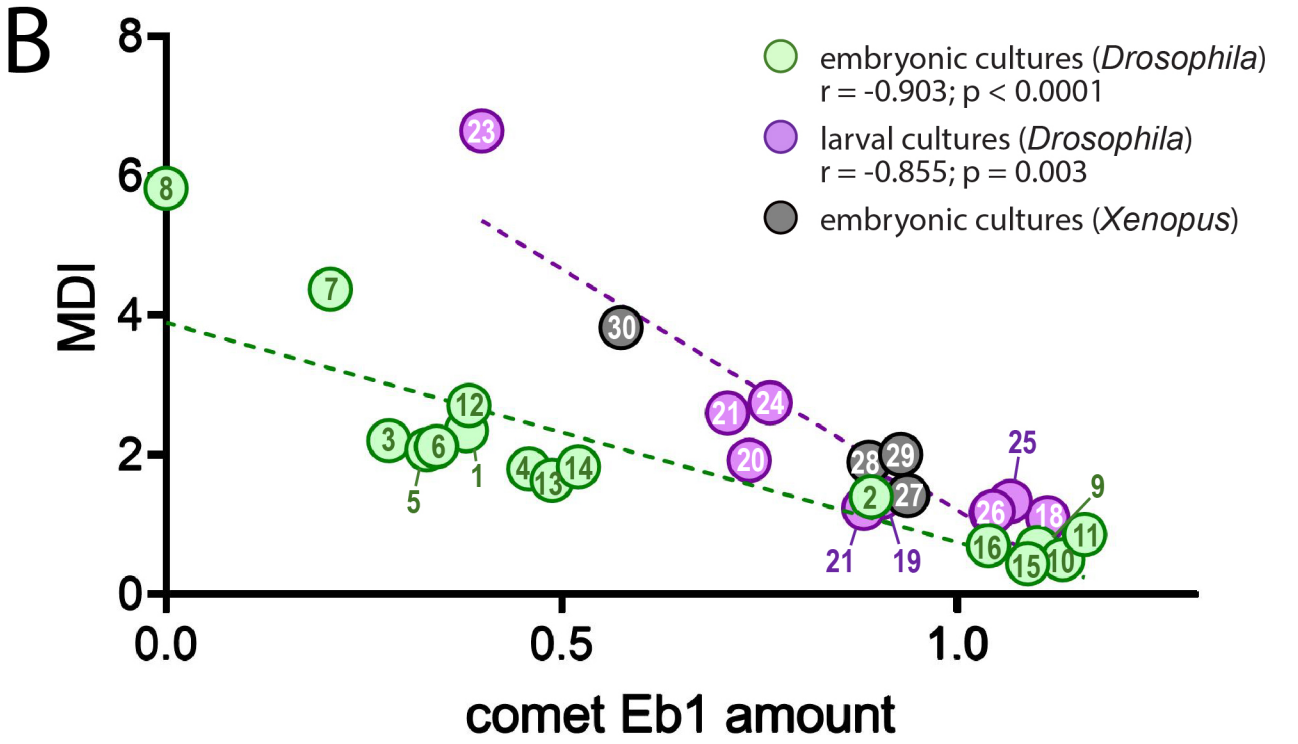
Hahn et al. Fig. 2

**A****B**

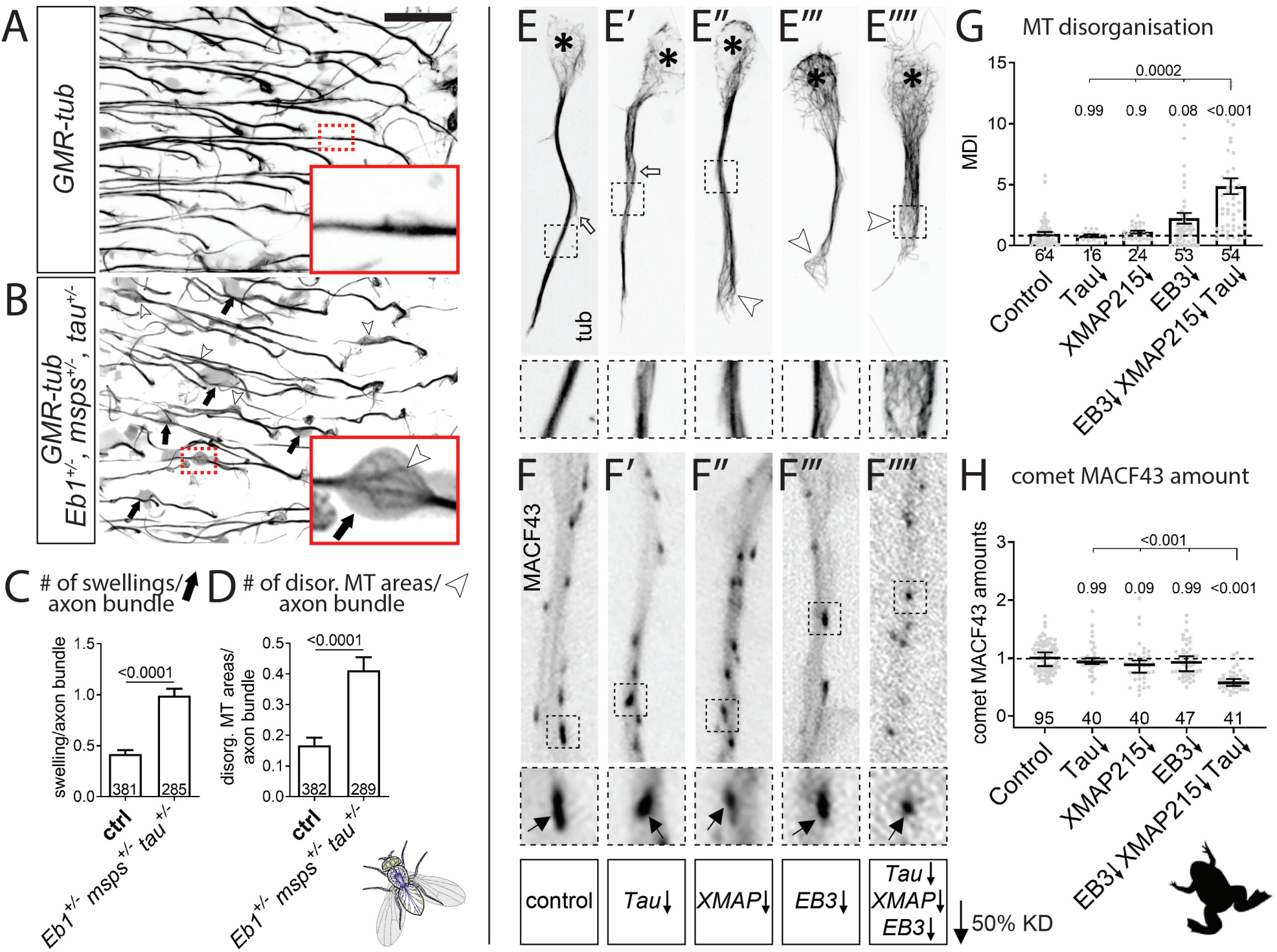
A

		comet Eb1 amount	MDI	Figure
1	6d pre <i>msps</i> <sup>1/1</sup>	0.3796	2.338	Fig. XXX1
2	6d pre <i>tau</i> <sup>KO/KO</sup>	0.8918	1.388	Fig. XXX1
3	6d pre <i>Eb1</i> <sup>04524/04524</sup>	0.282	2.191	Fig. XXX1
4	6d pre <i>msps</i> <sup>1/1</sup> <i>tau</i> <sup>KO/KO</sup>	0.4592	1.786	Fig. XXX2
5	6d pre <i>Eb1</i> <sup>04524/04524</sup> <i>tau</i> <sup>KO/KO</sup>	0.3298	2.063	Fig. XXX2
6	6d pre <i>Eb1</i> <sup>04524/04524</sup> <i>msps</i> <sup>1/1</sup>	0.3421	2.109	Fig. XXX2
7	6d pre <i>Eb1</i> <sup>04524/04524</sup> <i>msps</i> <sup>1/1</sup> <i>tau</i> <sup>KO/KO</sup>	0.2077	4.363	Fig. XXX2
8	7d pre <i>Eb1</i> <sup>Def</sup>	0	5.814	Fig. XXX2
9	6d pre <i>tub</i> <sup>def</sup>	1.102	0.6603	Fig. XXX1-S1
10	6d pre <i>clasp</i> <sup>2/Df</sup>	1.134	0.4888	Fig. XXX1-S1
11	6d pre <i>MAP1B</i> <sup>-</sup>	1.162	0.8491	Fig. XXX1-S1
12	6HIV <i>Eb1</i> <sup>04524</sup>	0.3832	2.697	Fig. XXX1-S1
13	6HIV <i>msps</i> <sup>A</sup>	0.4884	1.622	Fig. XXX1-S1
14	6HIV <i>tau</i> <sup>KO</sup>	0.5217	1.815	Fig. XXX1-S1
15	6HIV <i>tub</i> <sup>Df</sup>	1.09	0.43	Fig. XXX1-S1
16	6HIV <i>stai</i> <sup>KO1</sup>	1.04	0.69	Fig. XXX1-S1
17	L3 <i>msps</i> <sup>1/+</sup>	1.043	1.176	Fig. XXX2
18	L3 <i>tau</i> <sup>KO/+</sup>	1.114	1.11	Fig. XXX2
19	L3 <i>Eb1</i> <sup>04524/+</sup>	0.9031	1.397	Fig. XXX2
20	L3 <i>msps</i> <sup>1/+</sup> <i>tau</i> <sup>KO/+</sup>	0.7372	1.932	Fig. XXX2
21	L3 <i>tau</i> <sup>KO/+</sup> <i>Eb1</i> <sup>04524/+</sup>	0.8818	1.243	Fig. XXX2
22	L3 <i>msps</i> <sup>1/+</sup> <i>Eb1</i> <sup>04524/+</sup>	0.7095	2.609	Fig. XXX2
23	L3 <i>msps</i> <sup>1/+</sup> <i>tau</i> <sup>KO/+</sup> <i>Eb1</i> <sup>04524/+</sup>	0.399	6.655	Fig. XXX2
24	L3 <i>elavG4</i> ; <i>tau</i> <sup>KO/def</sup>	0.7631	2.758	Fig. XXX5
25	L3 <i>elav</i> > <i>EB1</i> -GFP, <i>tau</i> <sup>KO/def</sup>	1.067	1.34	Fig. XXX5
26	L3 <i>stai</i> <sup>Df/KO3</sup>	1.045	1.197	Fig. XXX1-S1
27	Xen 50% Tau KD	0.9358	1.411	Fig. XXX3
28	Xen 50% XMAP215 KD	0.8873	1.892	Fig. XXX3
29	Xen 50% EB3 KD	0.9271	2.002	Fig. XXX3
30	Xen 50% XMAP215/Tau/EB3 KD	0.5739	3.822	Fig. XXX3

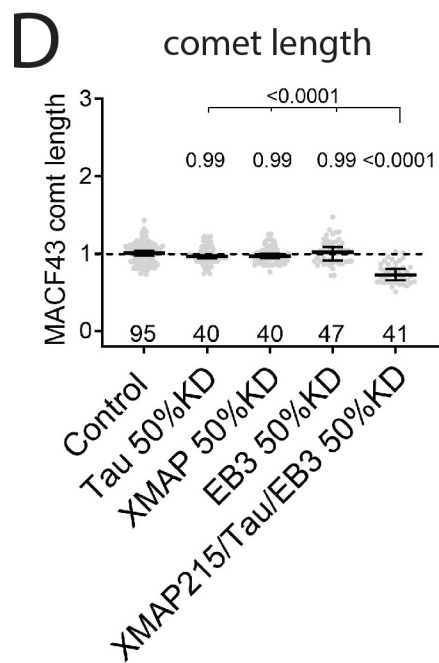
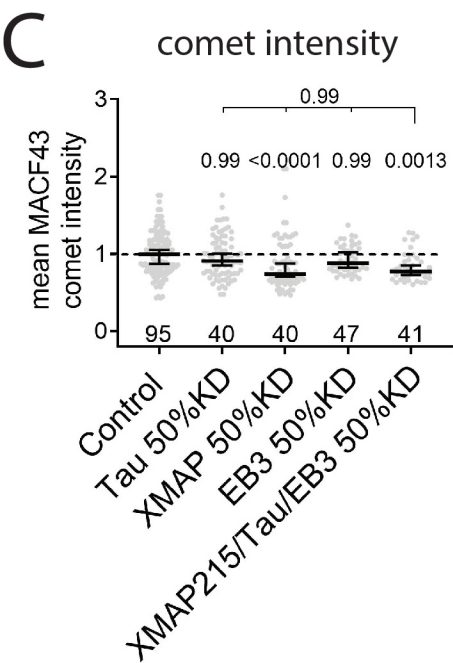
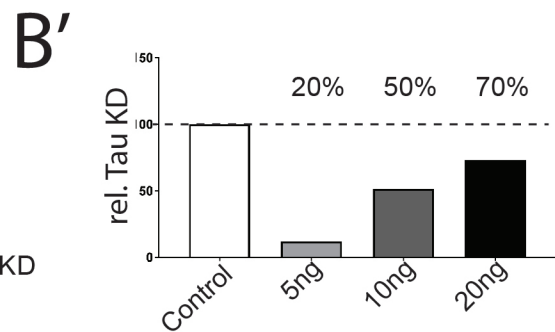
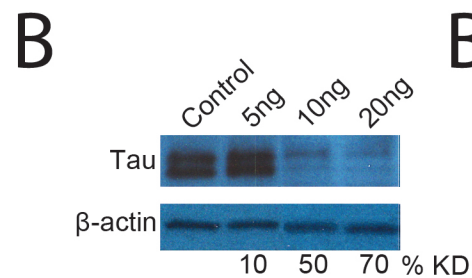
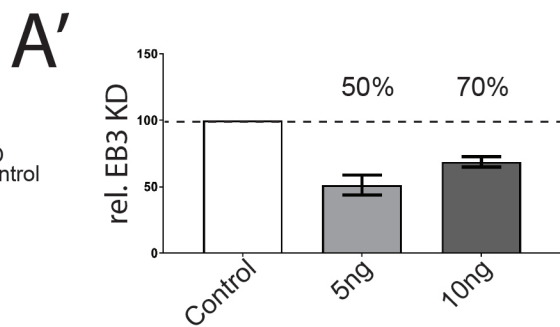
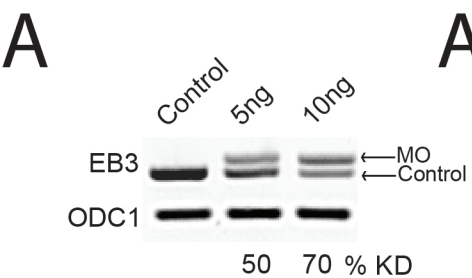
B

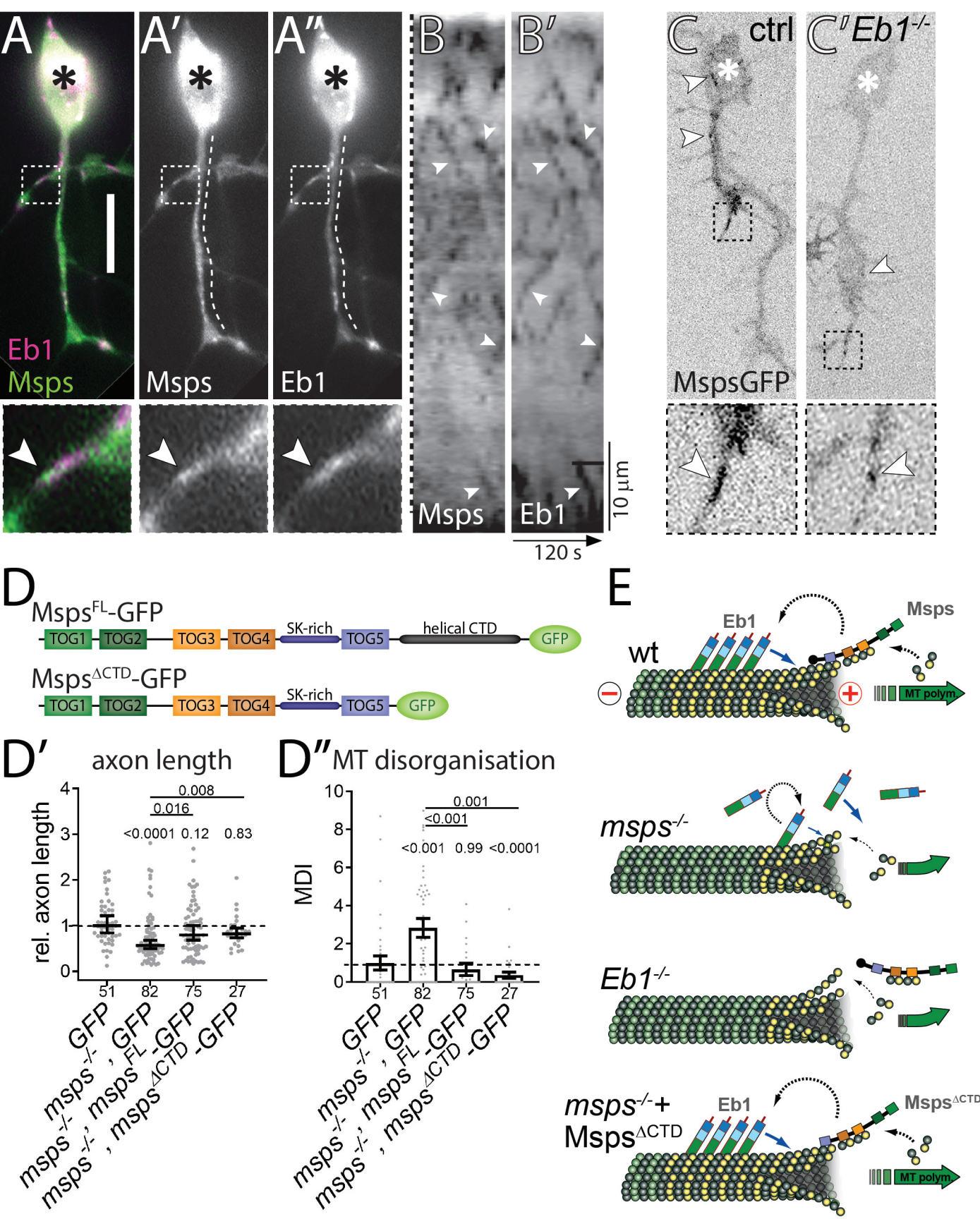












Hahn et al. Fig. 4

